Supporting information

Stereoregular polymerization of phenylacetylene by alkynyl and methyl rhodium(I) complexes with functionalized phosphine ligands: linear vs branched poly(phenylacetylene)s

Marta Angoy [a], M. Victoria Jiménez [a], Eugenio Vispe [a], Stepan Podzimek [b,c,d] and Jesús J. Pérez-Torrente [a]

[a] *Departamento de Química Inorgánica, Instituto de Síntesis Química y Catálisis Homogénea–ISQCH, Universidad de Zaragoza–CSIC, Facultad de Ciencias, C/ Pedro Cerbuna, 12, 50009 Zaragoza, Spain.*

[b] *Institute of Chemistry and Technology of Macromolecular Materials, Faculty of Chemical Technology, University of Pardubice, Pardubice, Czech Republic.*

[c] *Waters | Wyatt Technology, D-56307 Dernbach, Germany.*

[d] *SYNPO, 53207 Pardubice, Czech Republic.*

Email: perez@unizar.es

Content

1.- NMR spectra of alkynyl and methyl rhodium complexes having N- and O-functionalized phosphino ligands.

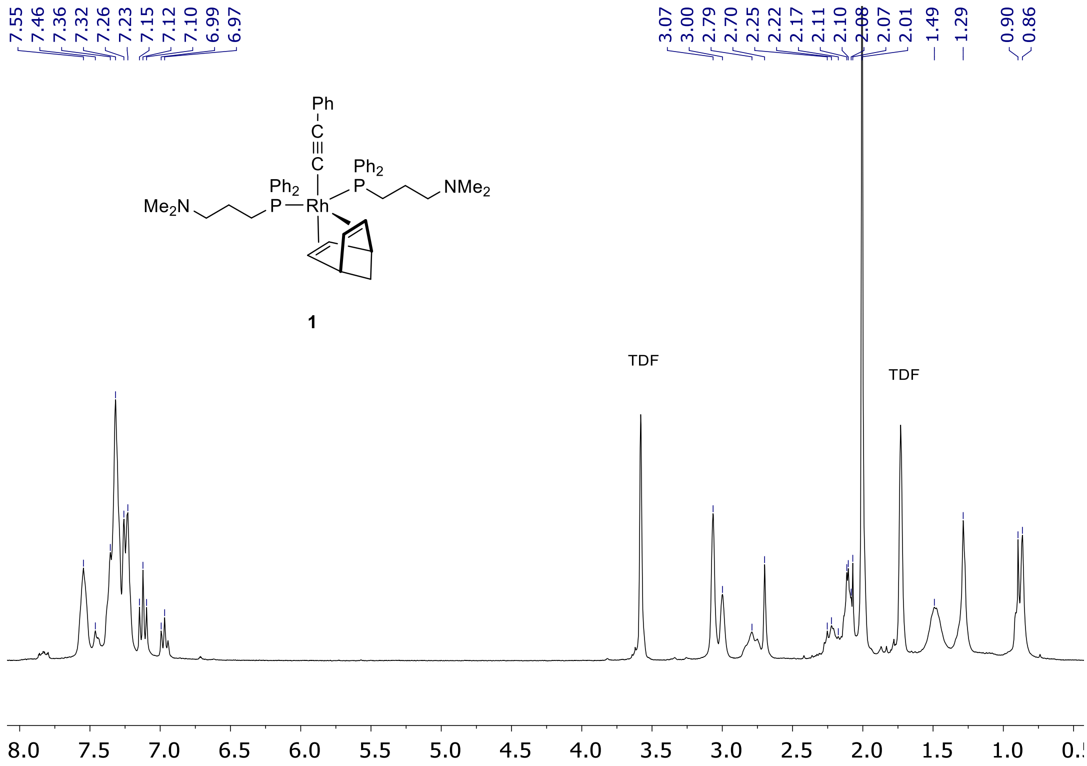

Figure S1. [1]H NMR (300 MHz, THF-d_8, 253 K) of [Rh(C≡C-Ph)(nbd){$Ph_2P(CH_2)_3NMe_2$}$_2$] (**1**).

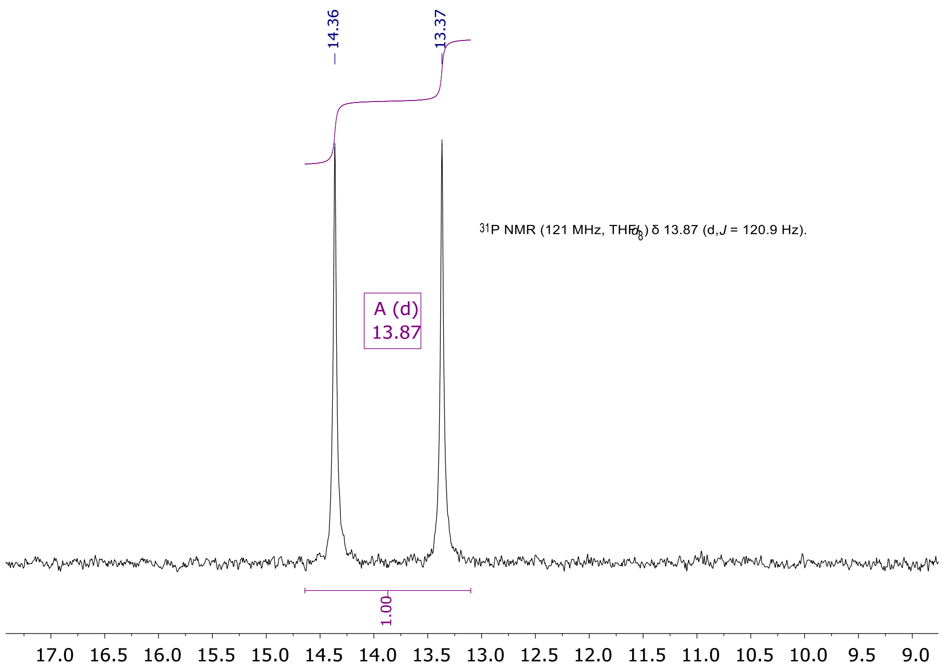

Figure S2. $^{31}P\{^1H\}$ NMR (121 MHz, THF-d_8, 253 K) of [Rh(C≡C-Ph)(nbd){$Ph_2P(CH_2)_3NMe_2$}$_2$] (**1**).

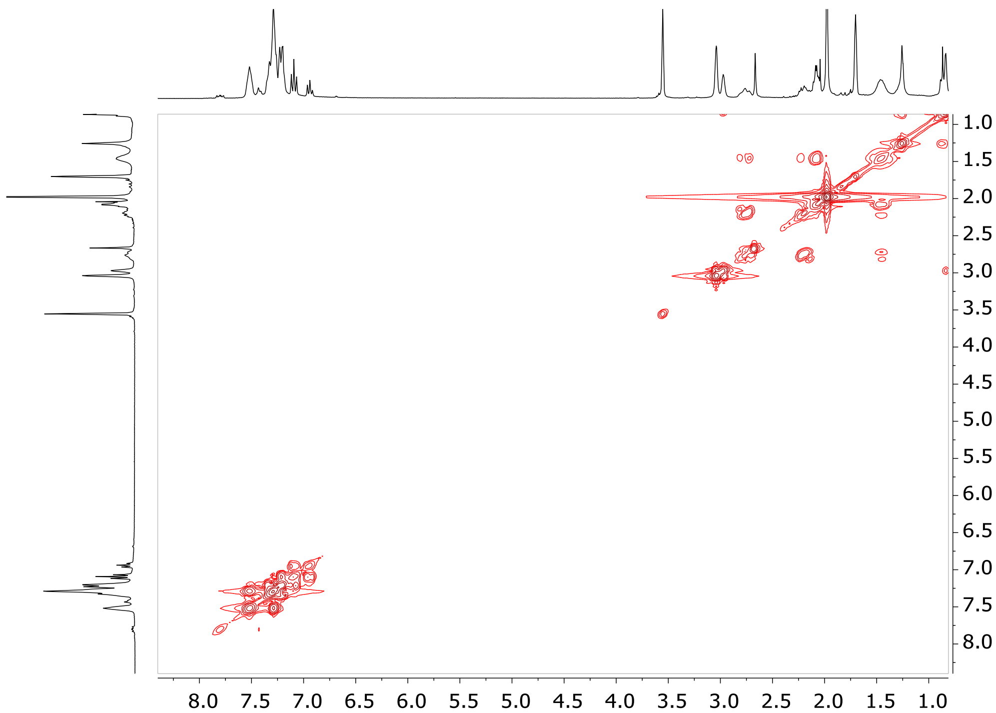

Figure S3. [1]H/[1]H-COSY NMR (THF-d_8, 253 K) of [Rh(C≡C-Ph)(nbd){$Ph_2P(CH_2)_3NMe_2$}$_2$] (**1**).

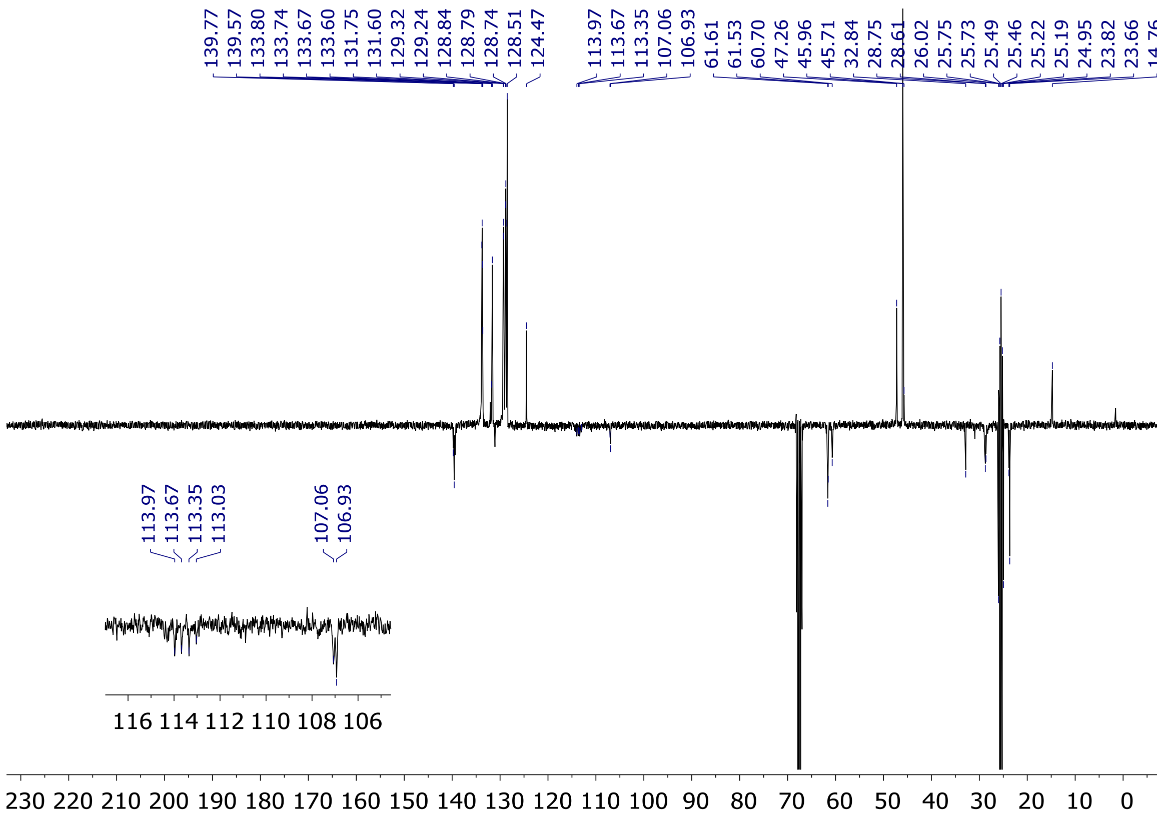

Figure S4. [13]C{[1]H} NMR (75 MHz, THF-d_8, 253 K) of [Rh(C≡C-Ph)(nbd){$Ph_2P(CH_2)_3NMe_2$}$_2$] (**1**).

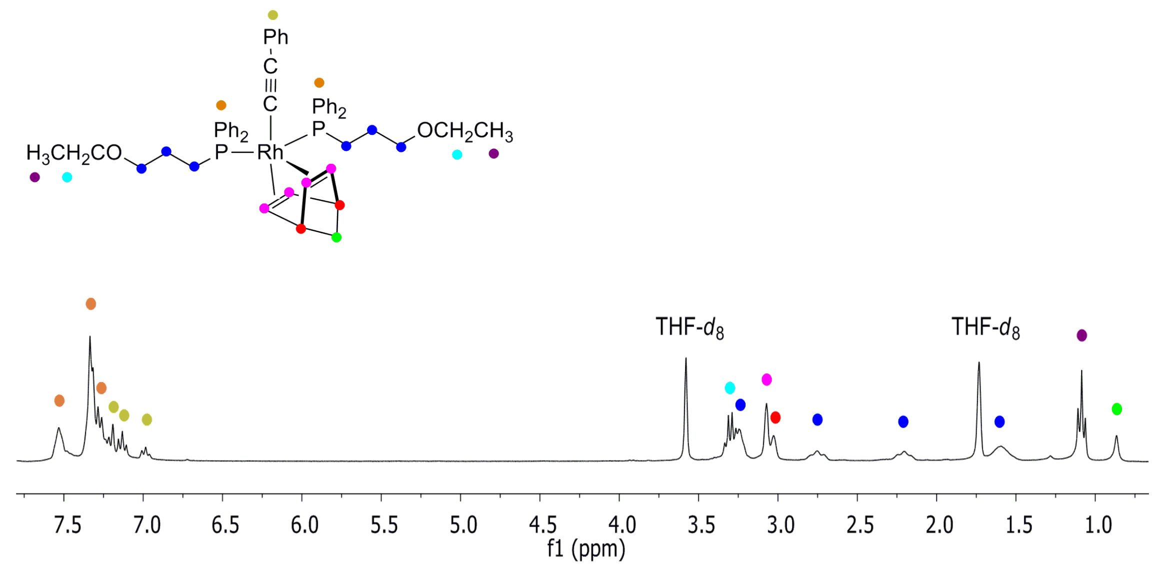

Figure S5. ^{1}H NMR (300 MHz, THF-d_8, 253 K) of [Rh(C≡C-Ph)(nbd){$Ph_2P(CH_2)_3OEt$}$_2$] (**2**).

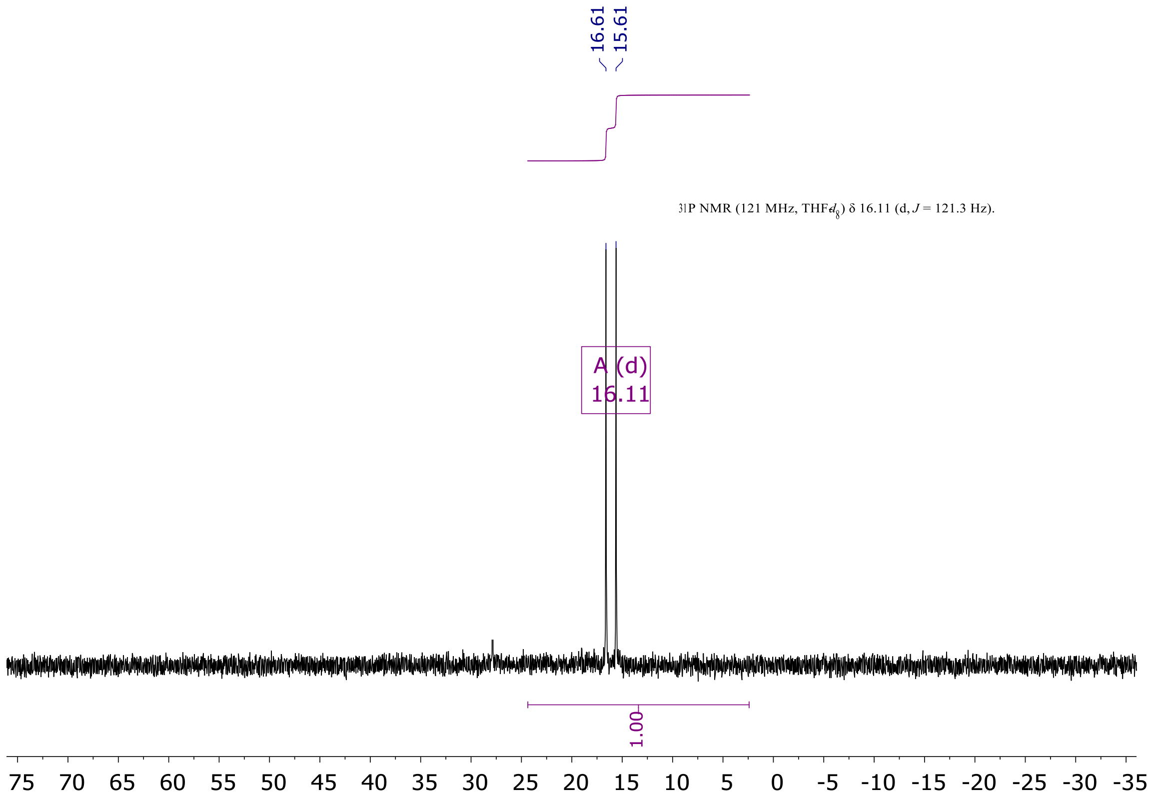

Figure S6. ^{31}P{^{1}H} NMR (300 MHz, THF-d_8, 253 K) of [Rh(C≡C-Ph)(nbd){$Ph_2P(CH_2)_3OEt$}$_2$] (**2**).

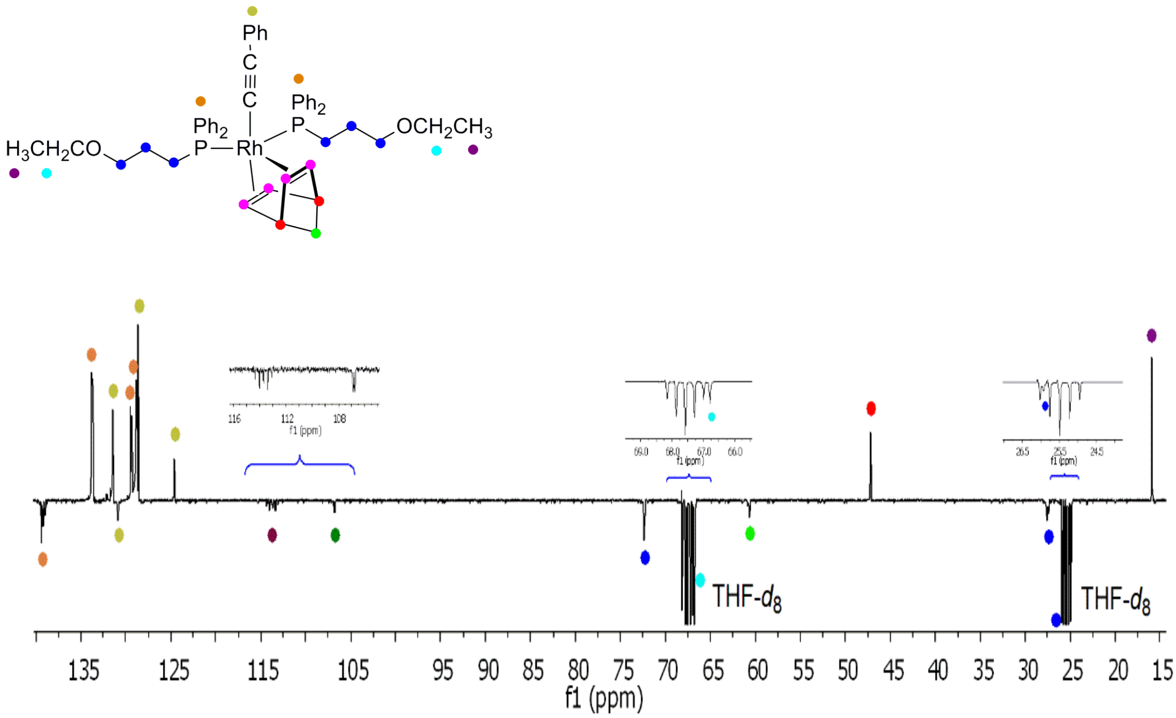

Figure S7. $^{13}C\{^{1}H\}$ NMR (75 MHz, THF-d_8, 253 K) of [Rh(C≡C-Ph)(nbd){$Ph_2P(CH_2)_3OEt$}$_2$] (**2**).

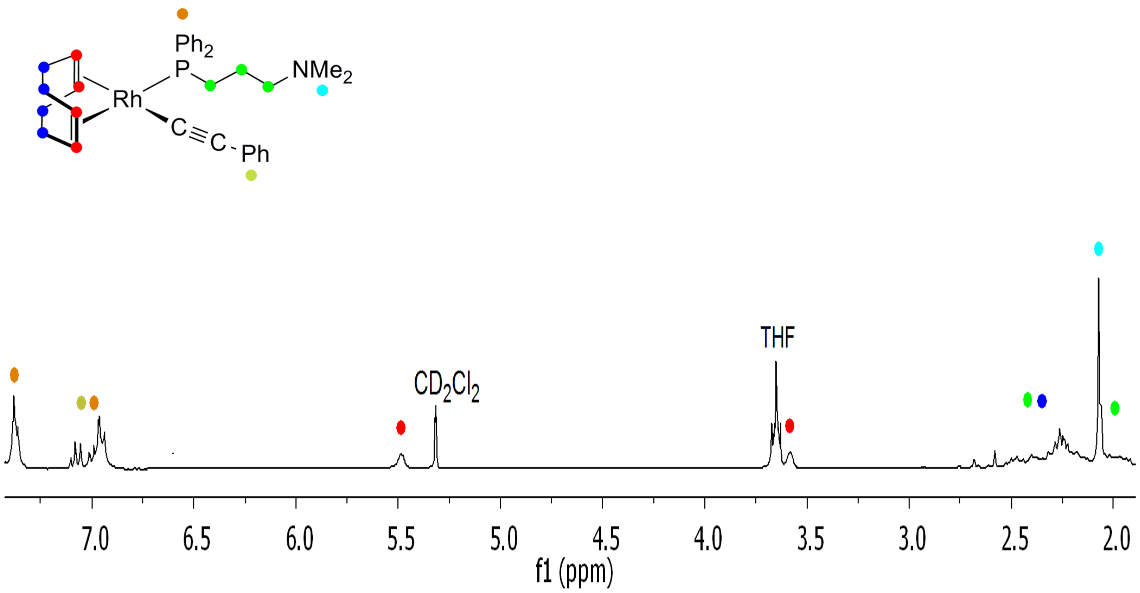

Figure S8. ^{1}H NMR (300 MHz, CD_2Cl_2, 233 K) of [Rh(C≡C-Ph)(cod){$Ph_2P(CH_2)_3NMe_2$}] (**3**).

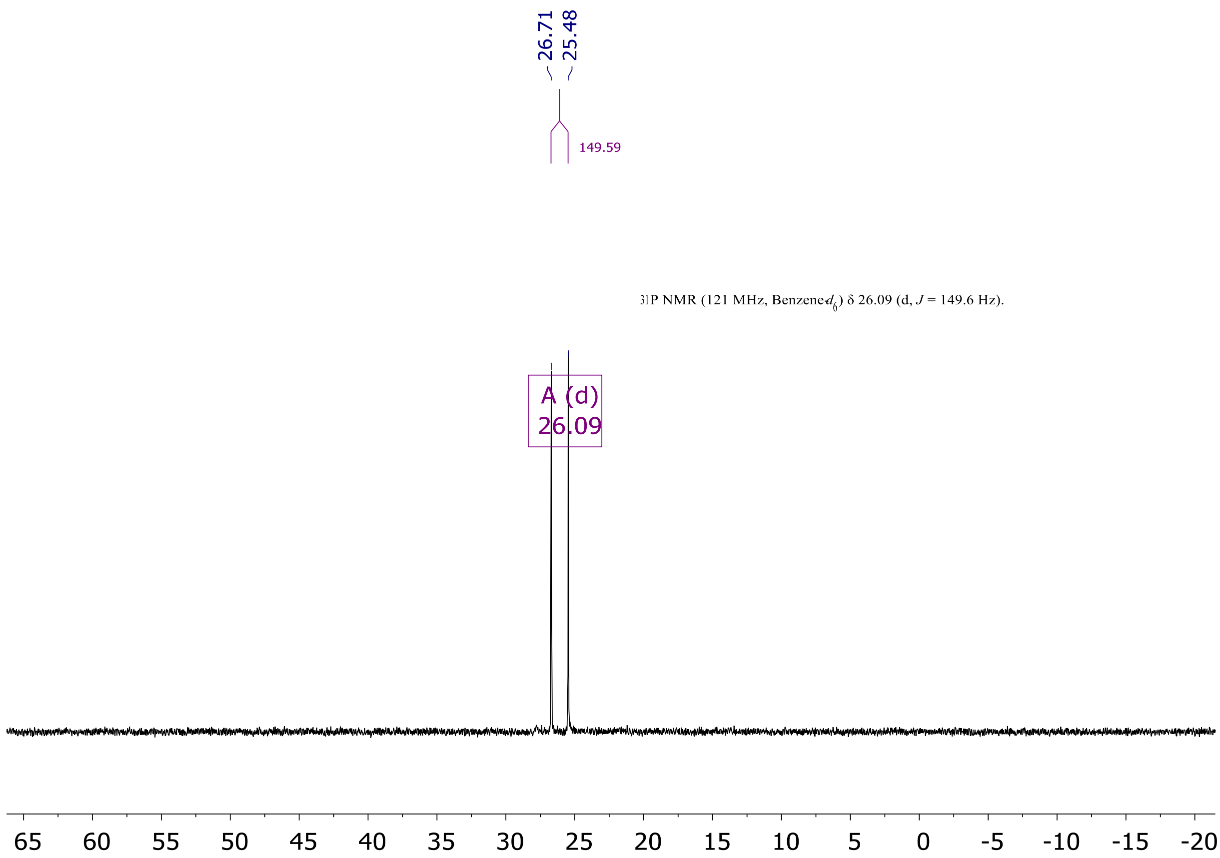

Figure S9. ^{31}P NMR (300 MHz, C_6D_6, 298 K) of [Rh(C≡C-Ph)(cod){$Ph_2P(CH_2)_3NMe_2$}] (**3**).

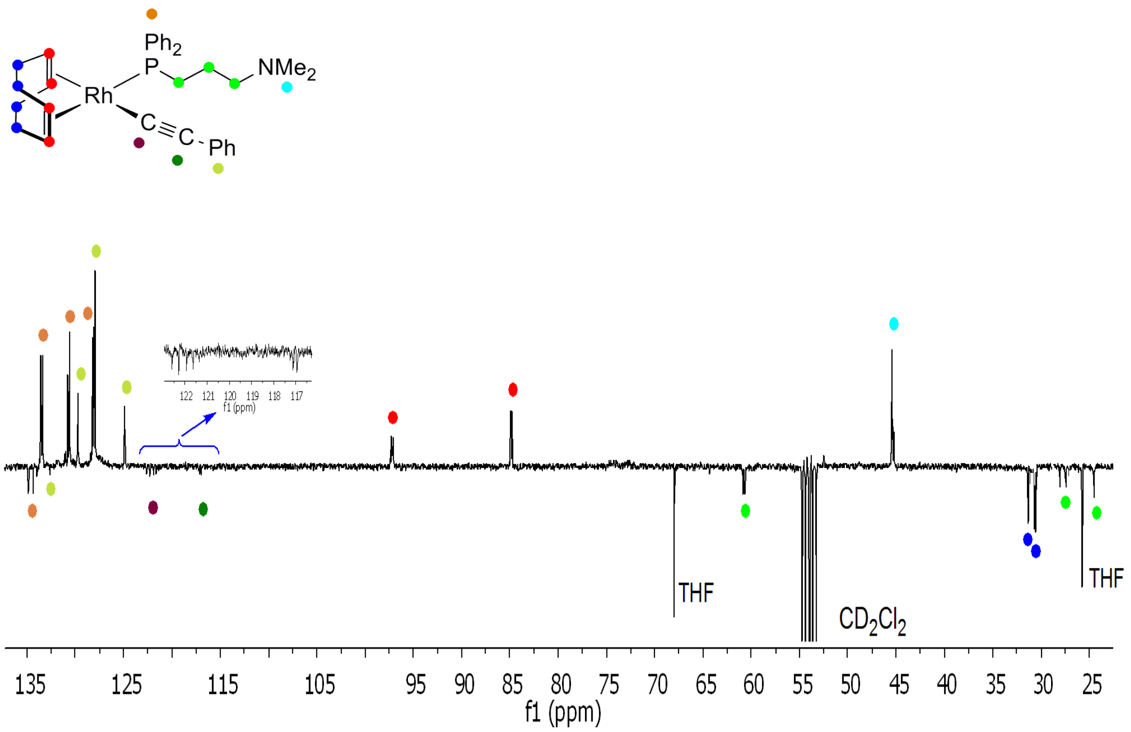

Figure S10. $^{13}C\{^{1}H\}$ NMR (75 MHz, CD_2Cl_2, 233 K) of [Rh(C≡C-Ph)(cod){$Ph_2P(CH_2)_3NMe_2$}] (**3**).

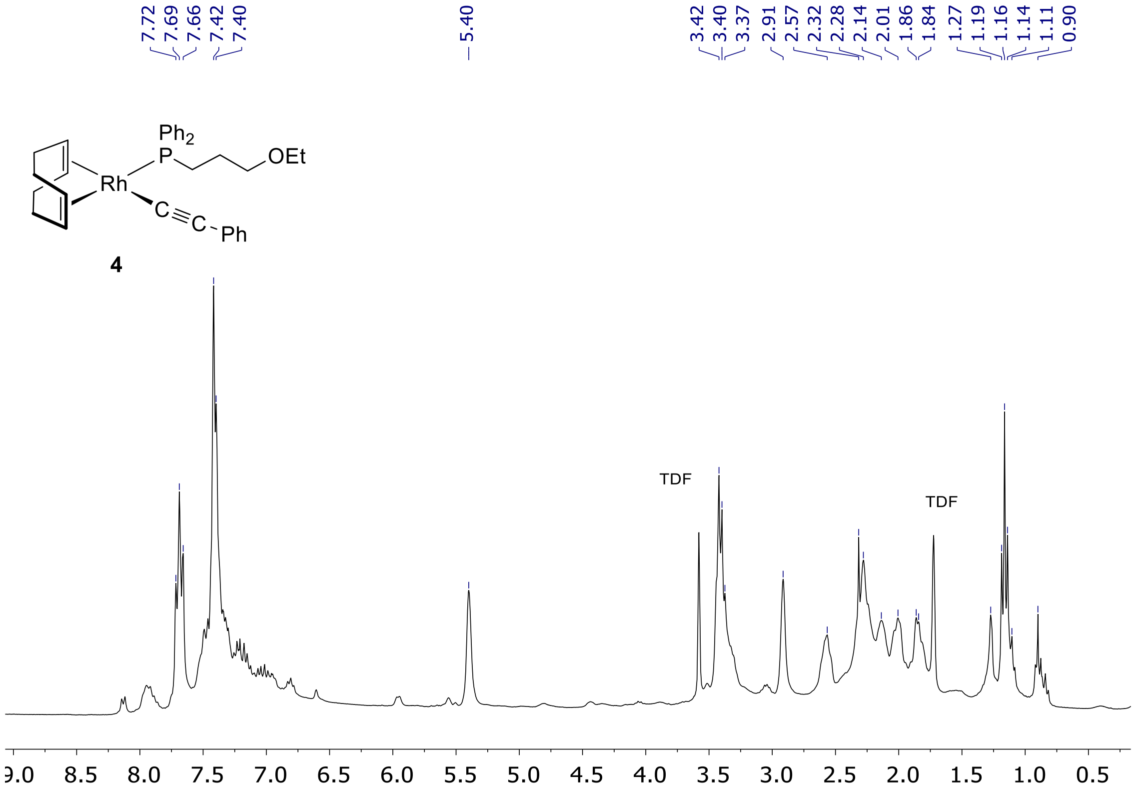

Figure S11. [1]H NMR (300 MHz, THF-d_8, 233 K) of [Rh(C≡C-Ph)(cod){$Ph_2P(CH_2)_3OEt$}] (**4**).

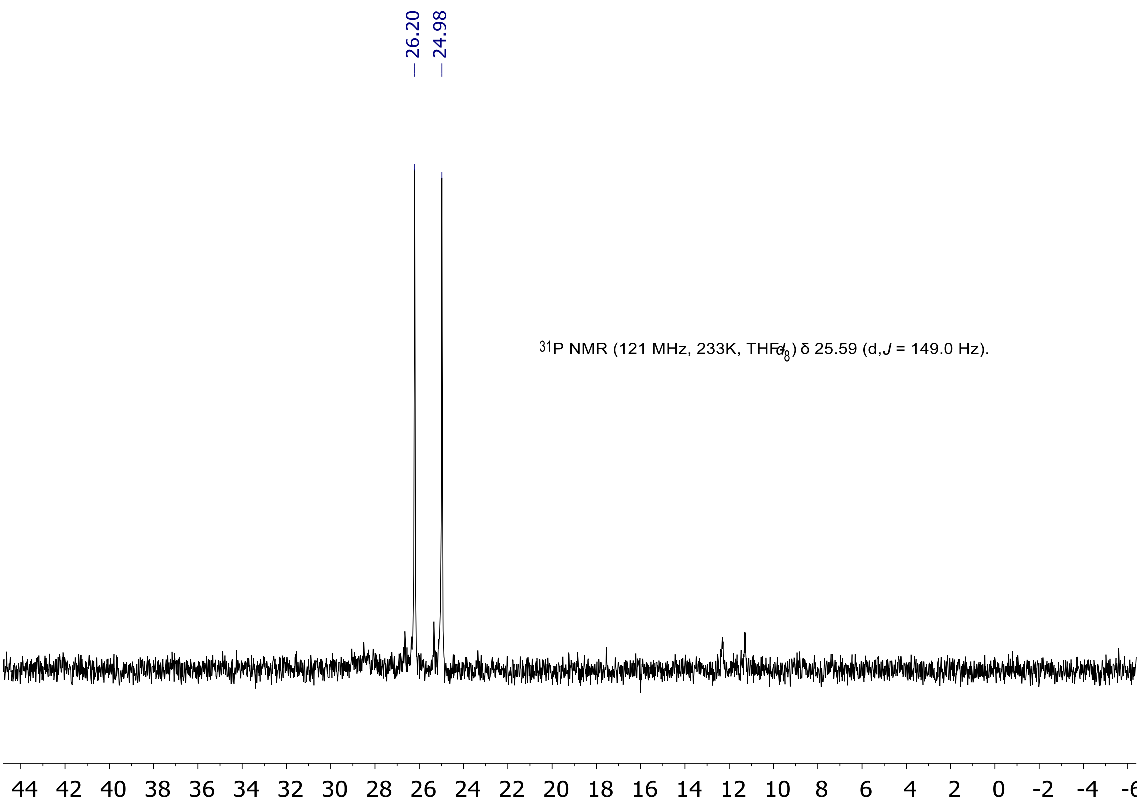

Figure S12. $^{31}P\{^1H\}$ NMR (121 MHz, THF-d_8, 233 K) of [Rh(C≡C-Ph)(cod){$Ph_2P(CH_2)_3OEt$}] (**4**).

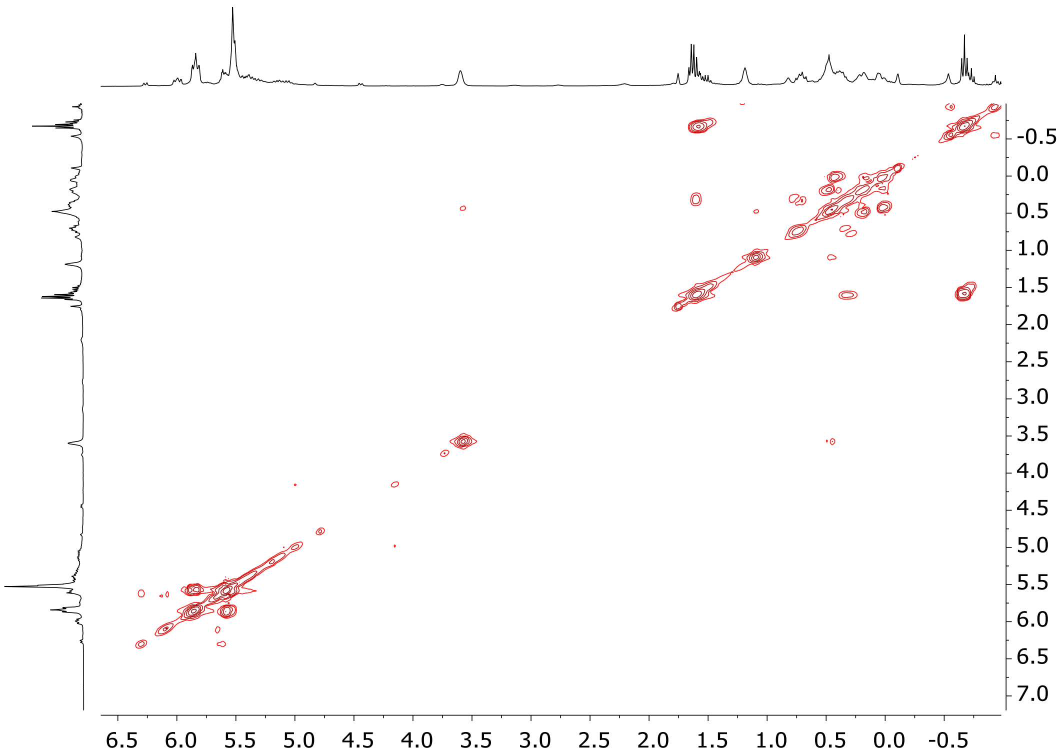

Figure S13.[1]H/[1]H-COSY NMR (THF-d_8, 233 K) of [Rh(C≡C-Ph)(cod){$Ph_2P(CH_2)_3OEt$}] (**4**).

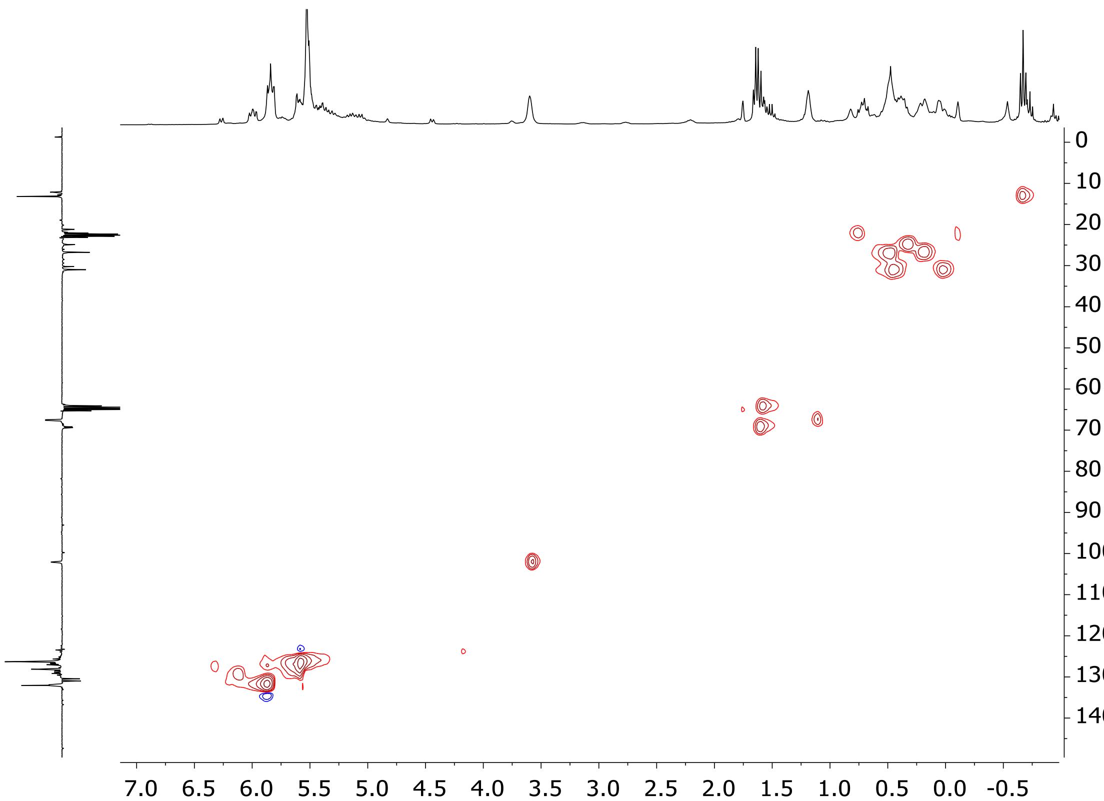

Figure S14.[1]H/[13]C HSQC NMR (THF-d_8, 233 K) of [Rh(C≡C-Ph)(cod){$Ph_2P(CH_2)_3OEt$}] (**4**).

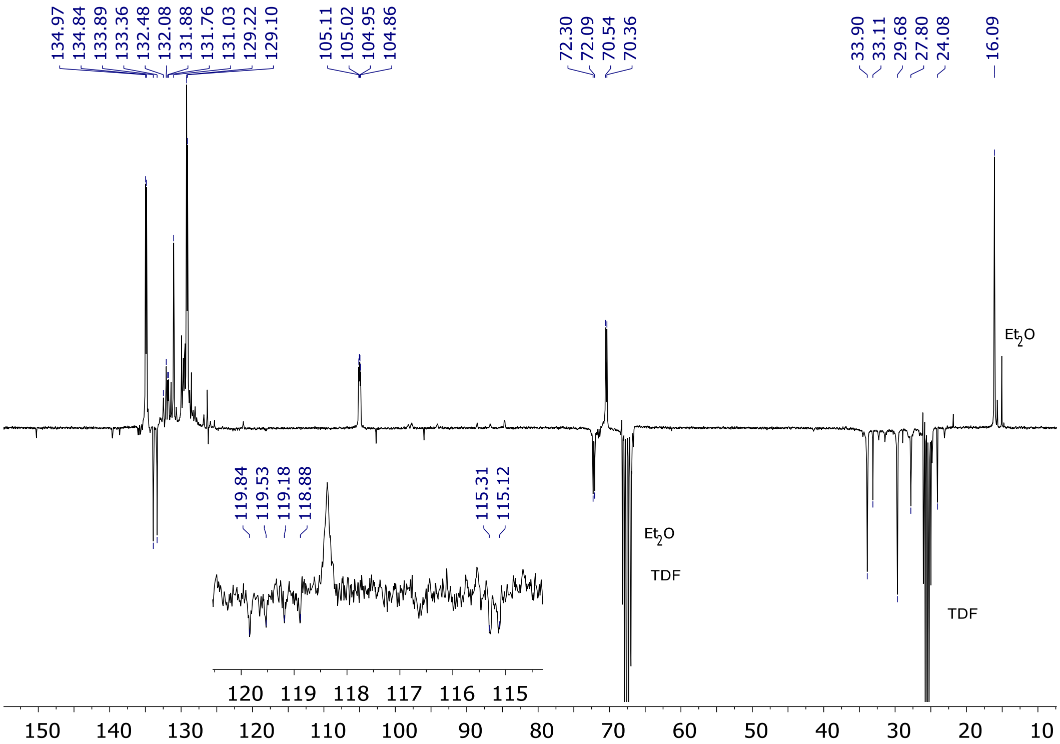

Figure S15. $^{13}C\{^1H\}$ NMR (75 MHz, THF-d_8, 233 K) of [Rh(C≡C-Ph)(cod){$Ph_2P(CH_2)_3OEt$}] (**4**).

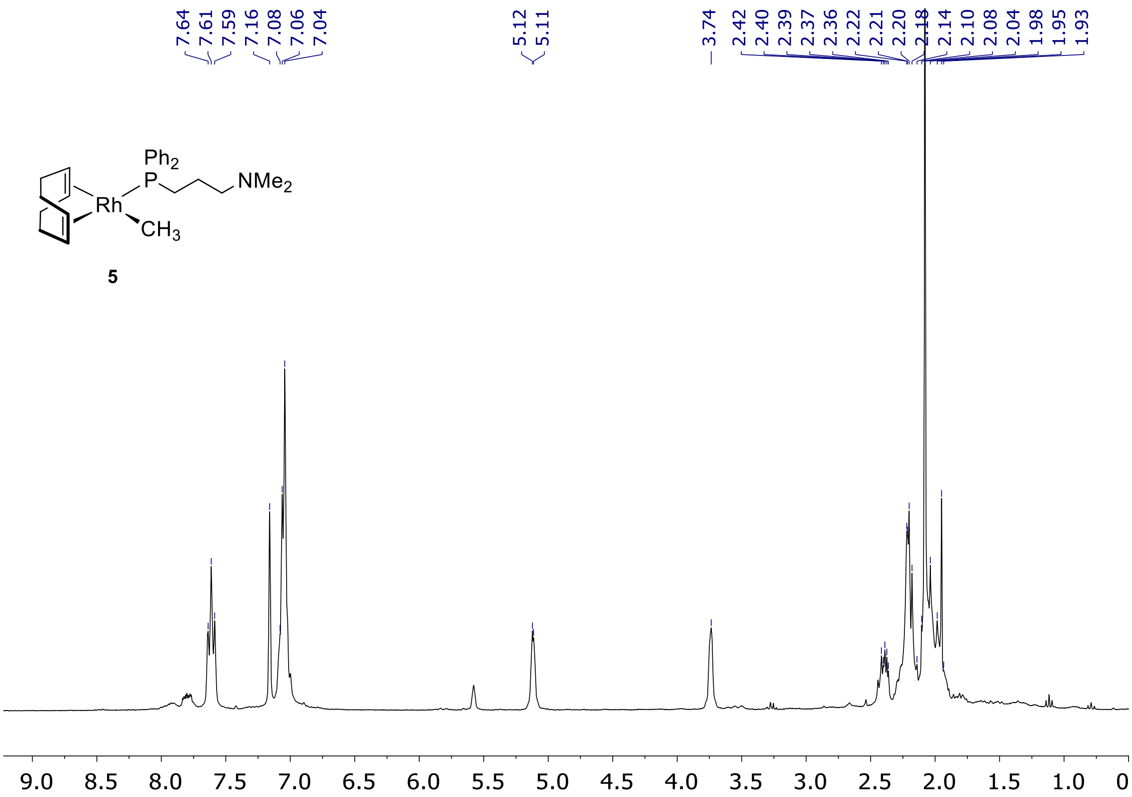

Figure S16.^1H NMR (300 MHz, C_6D_6, 298 K) of [Rh(CH_3)(cod){$Ph_2P(CH_2)_3NMe_2$}] (**5**).

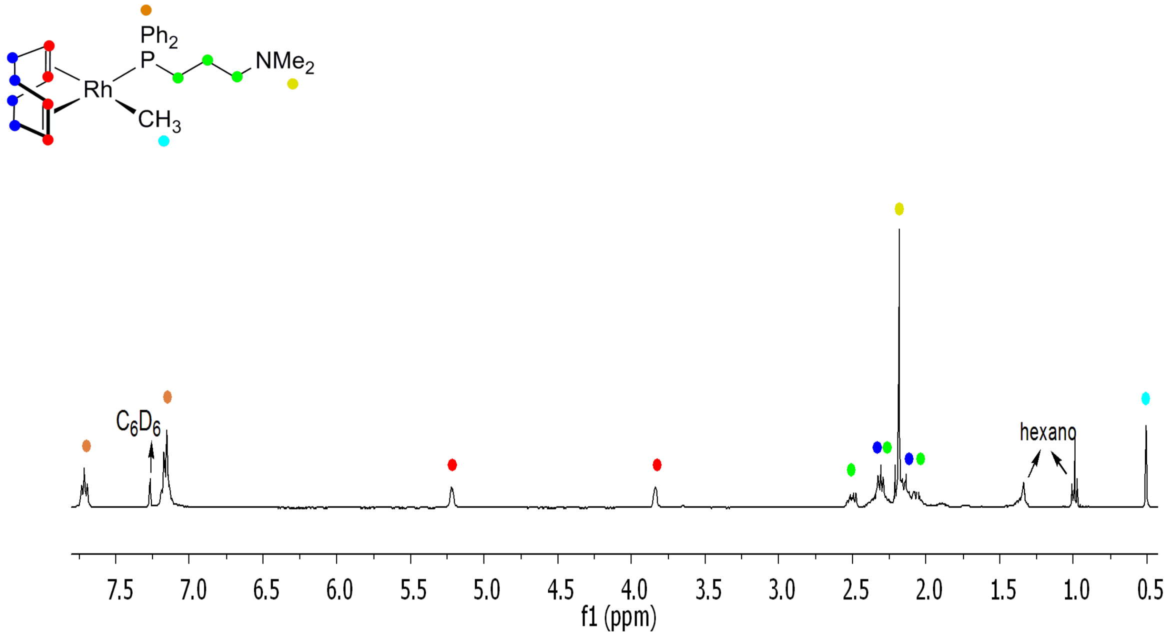

Figure S17. [1]H NMR (300 MHz, C_6D_6, 298 K) of [Rh(CH_3)(cod){$Ph_2P(CH_2)_3NMe_2$}] (**5**).

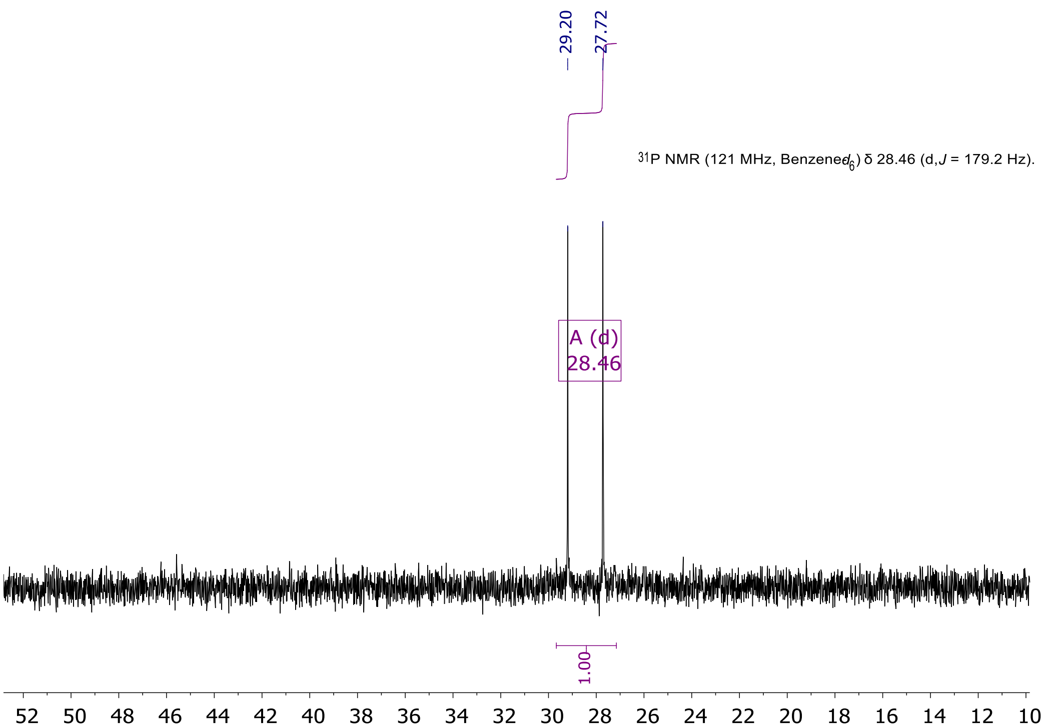

Figure S18.[31]P{[1]H} NMR (121 MHz, C_6D_6, 298 K) of [Rh(CH_3)(cod){$Ph_2P(CH_2)_3NMe_2$}] (**5**).

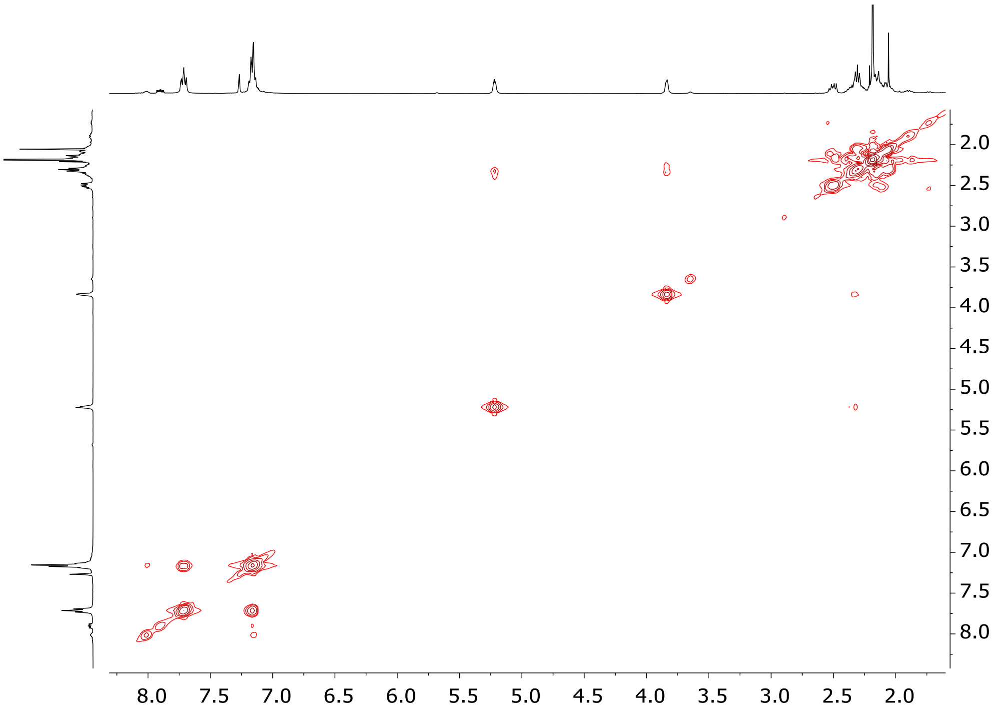

Figure S19. $^{1}H/^{1}H$-COSY NMR (C_6D_6, 298 K) of [Rh(CH_3)(cod){$Ph_2P(CH_2)_3NMe_2$}] (**5**).

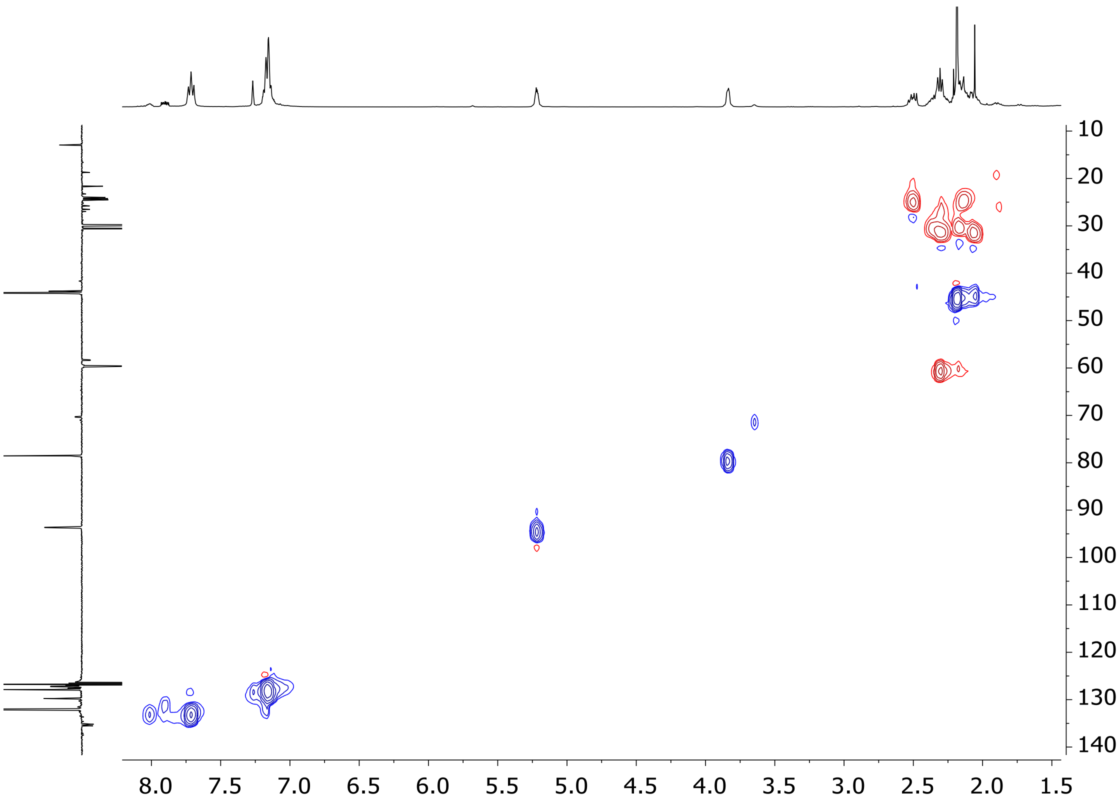

Figure S20. $^{1}H/^{13}C$ HSQC NMR (C_6D_6, 298 K) of [Rh(CH_3)(cod){$Ph_2P(CH_2)_3NMe_2$}](**5**).

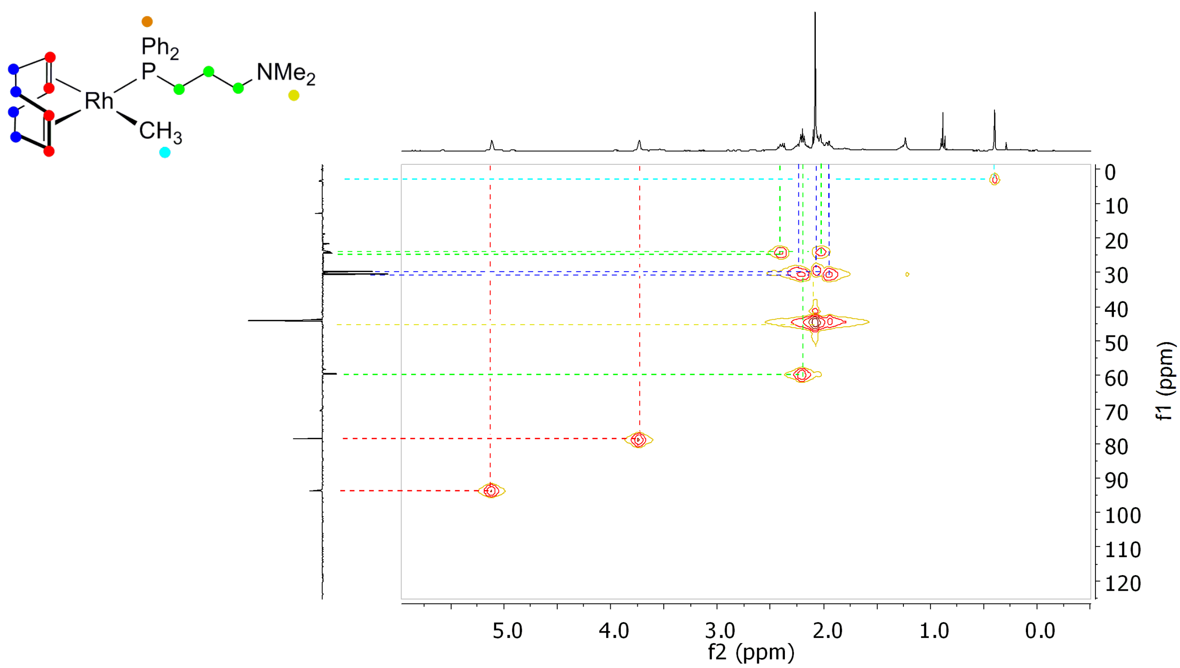

Figure S21. Expansion of the $^{1}H/^{13}C$ HSQC NMR (C_6D_6, 298 K) of **5** from 0 to 6 ppm in ^{1}H.

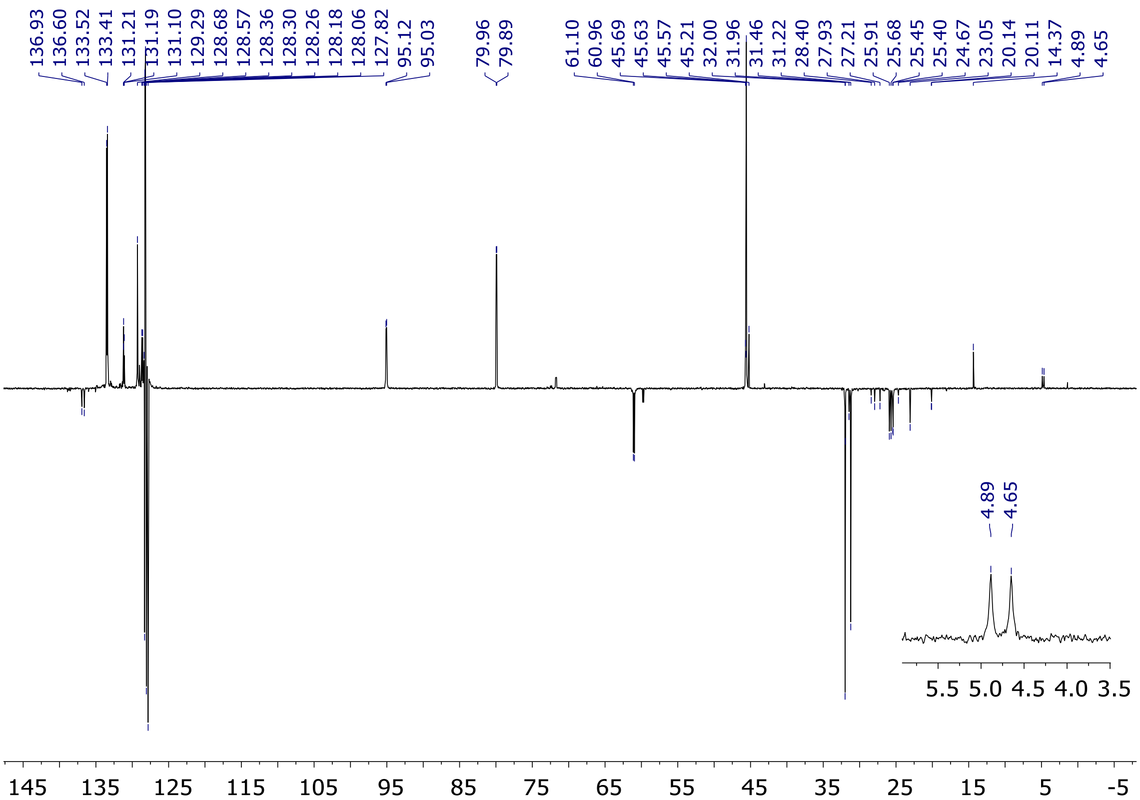

Figure S22. $^{13}C\{^{1}H\}$ NMR (75 MHz, C_6D_6, 298 K) of $[Rh(CH_3)(cod)\{Ph_2P(CH_2)_3NMe_2\}]$ (**5**).

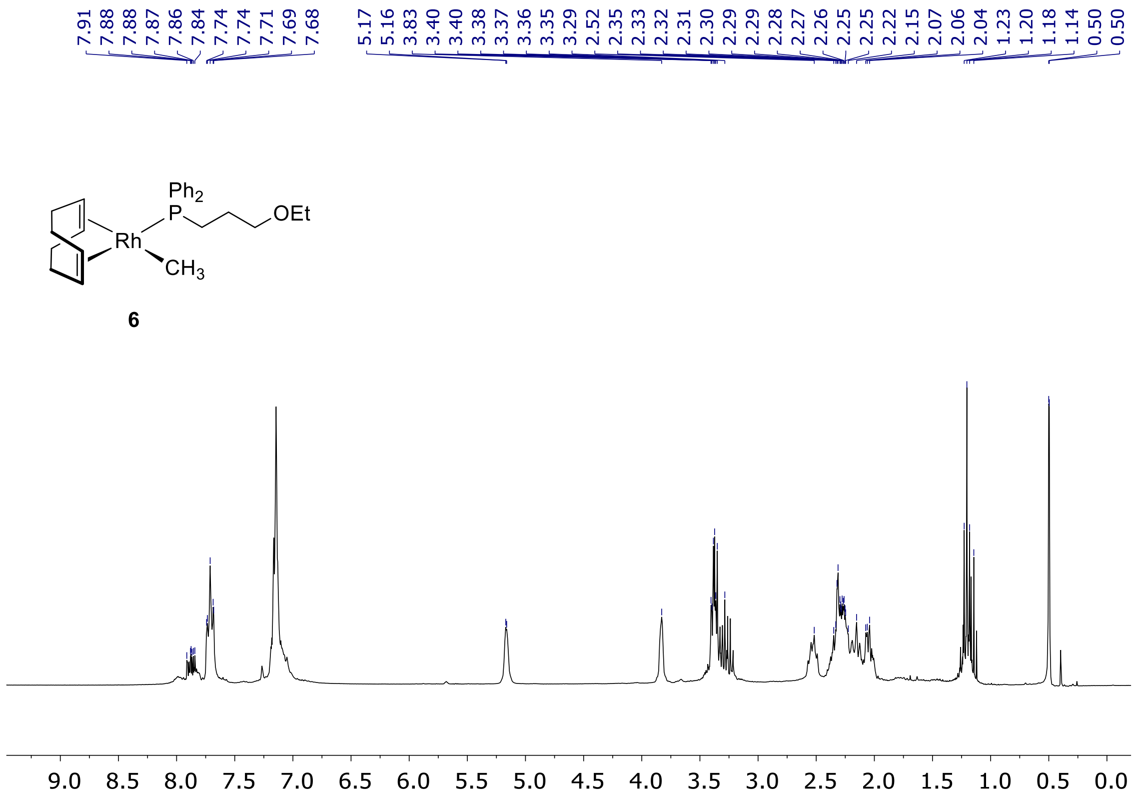

Figure S23.[1]H NMR (300 MHz, C_6D_6, 298 K) of [Rh(CH_3)(cod){$Ph_2P(CH_2)_3OEt$}] (**6**).

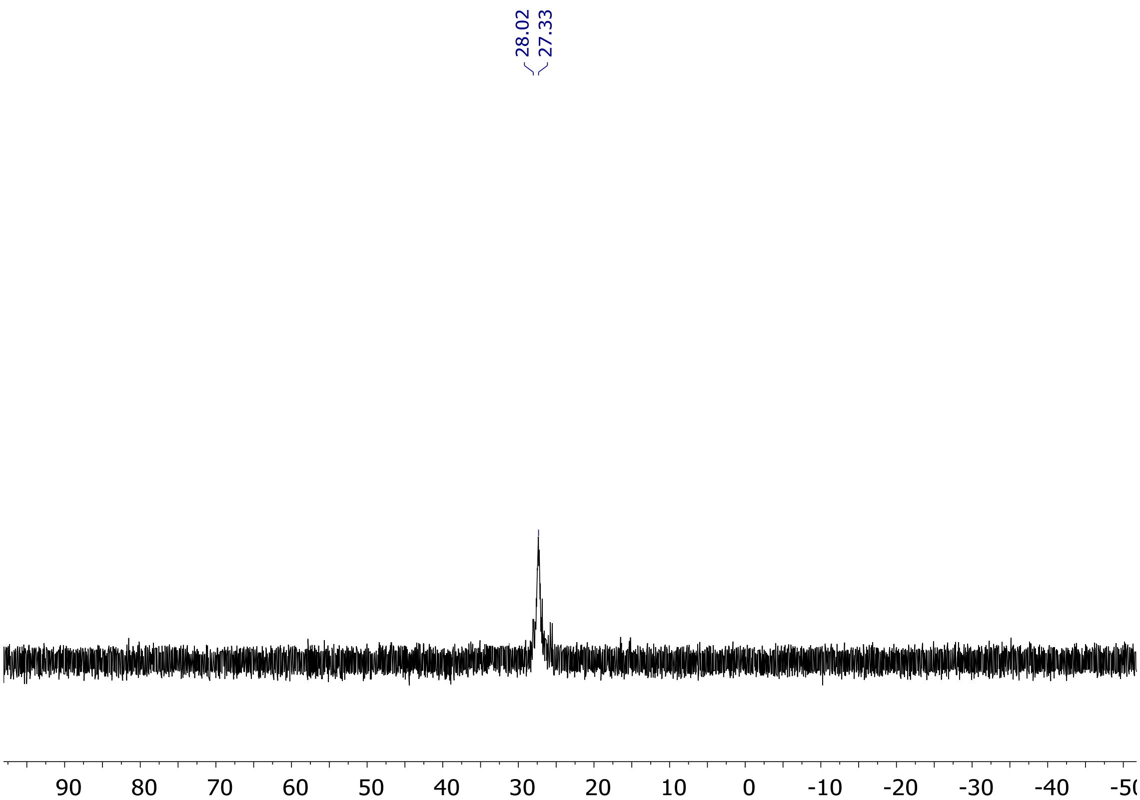

Figure S24.[31]P{[1]H} NMR (121 MHz, C_6D_6, 298 K) of [Rh(CH_3)(cod){$Ph_2P(CH_2)_3OEt$}] (**6**).

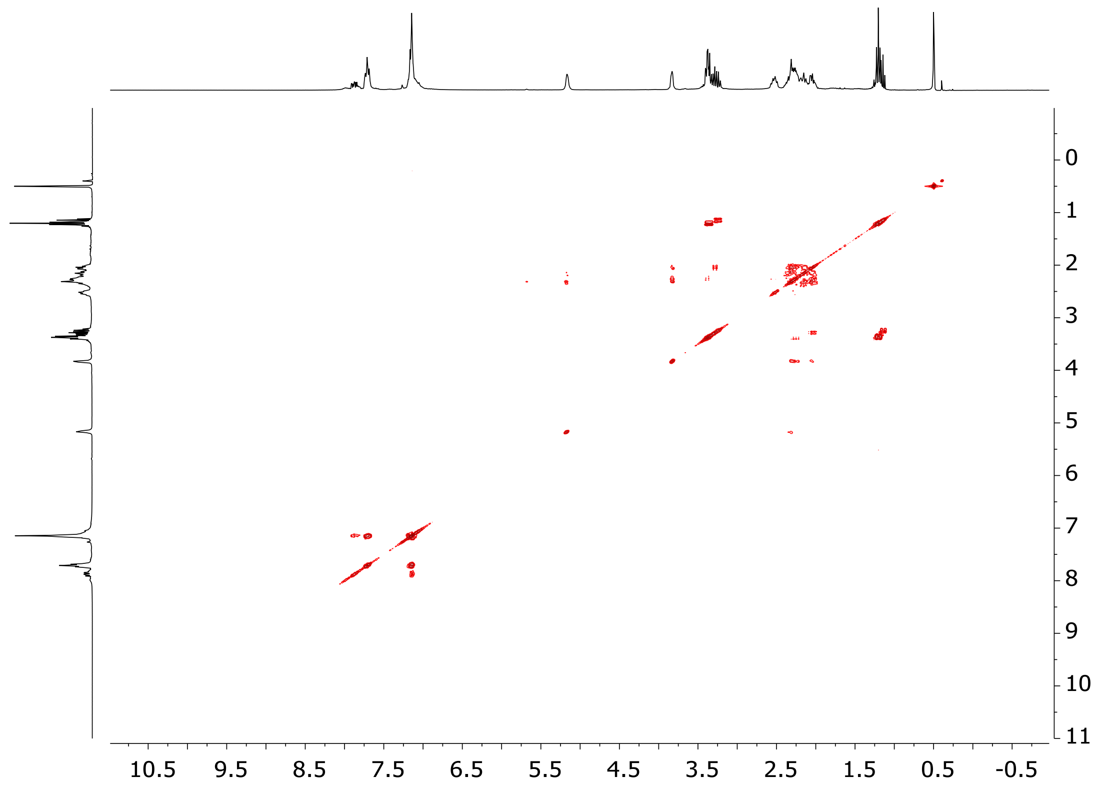

Figure S25. $^1H/^1H$-COSY NMR (C_6D_6, 298 K) of $[Rh(CH_3)(cod)\{Ph_2P(CH_2)_3OEt\}]$ (**6**).

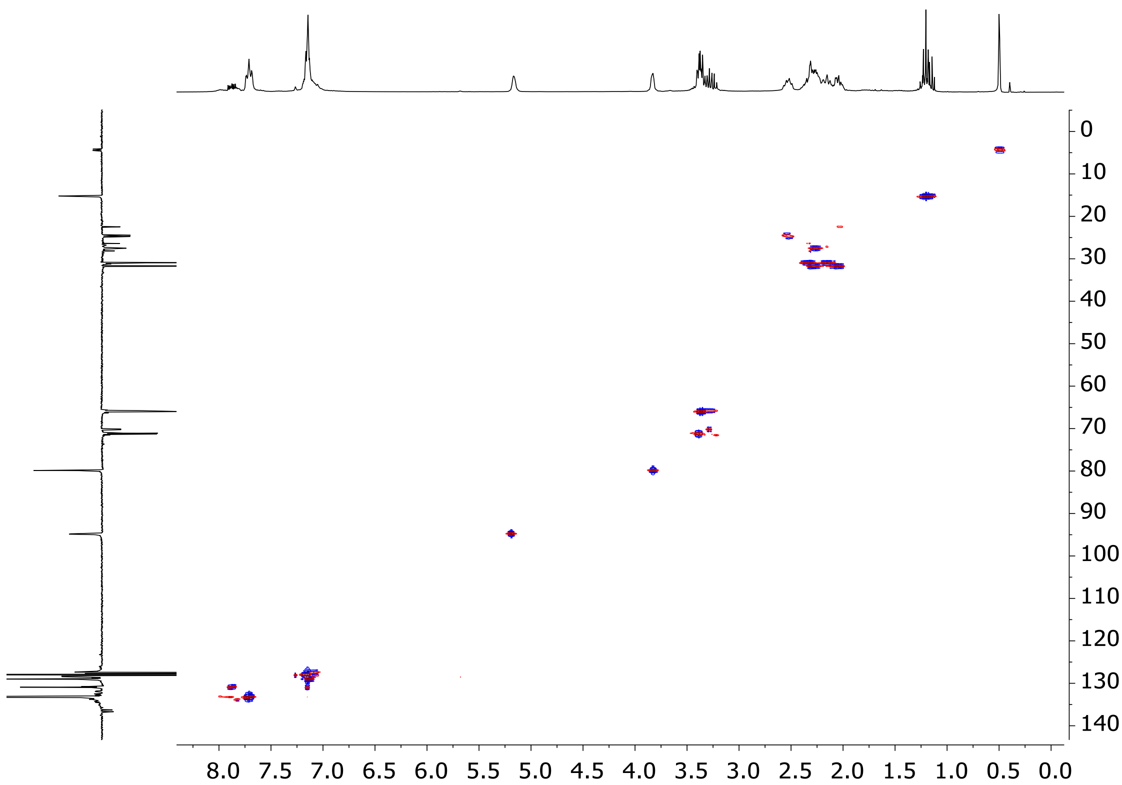

Figure S26. $^1H/^{13}C$ HSQC NMR (C_6D_6, 298 K) of $[Rh(CH_3)(cod)\{Ph_2P(CH_2)_3OEt\}]$ (**6**).

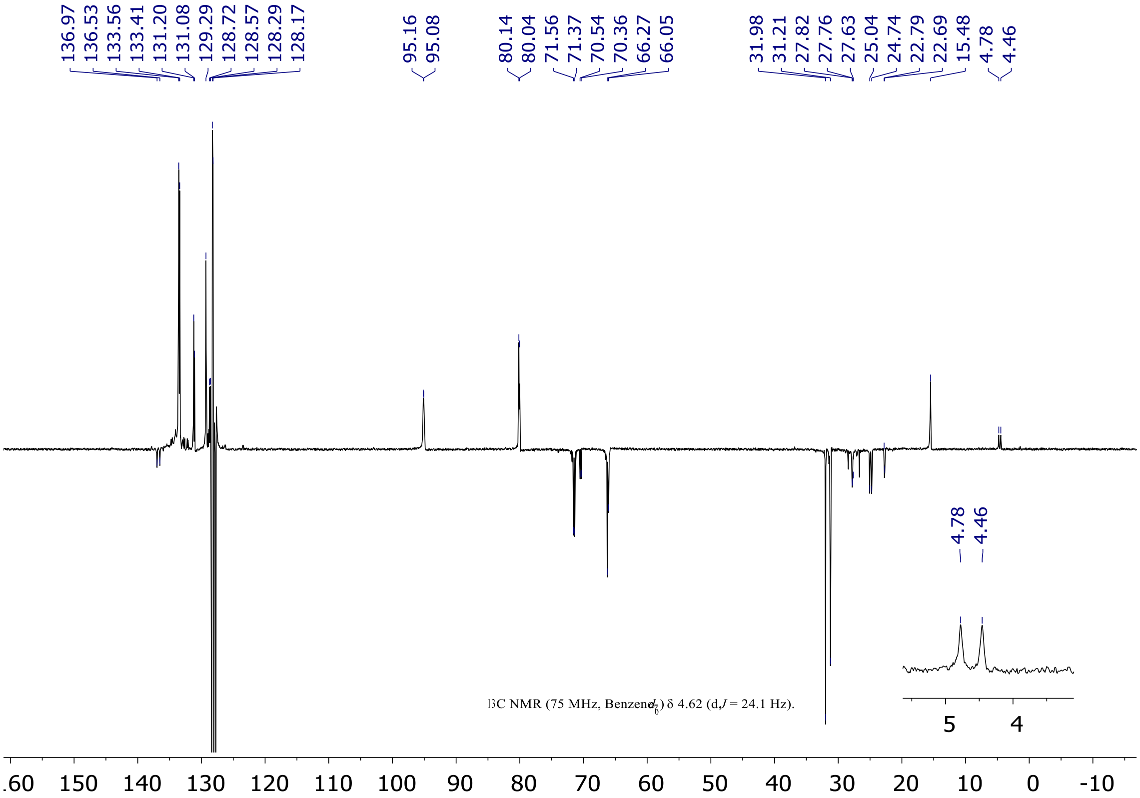

Figure S27. $^{13}C\{^{1}H\}$ NMR (75 MHz, C_6D_6, 298 K) of [Rh(CH_3)(cod){$Ph_2P(CH_2)_3OEt$}] (**6**).

2.- ESI-MS of alkynyl and methyl rhodium complexes.

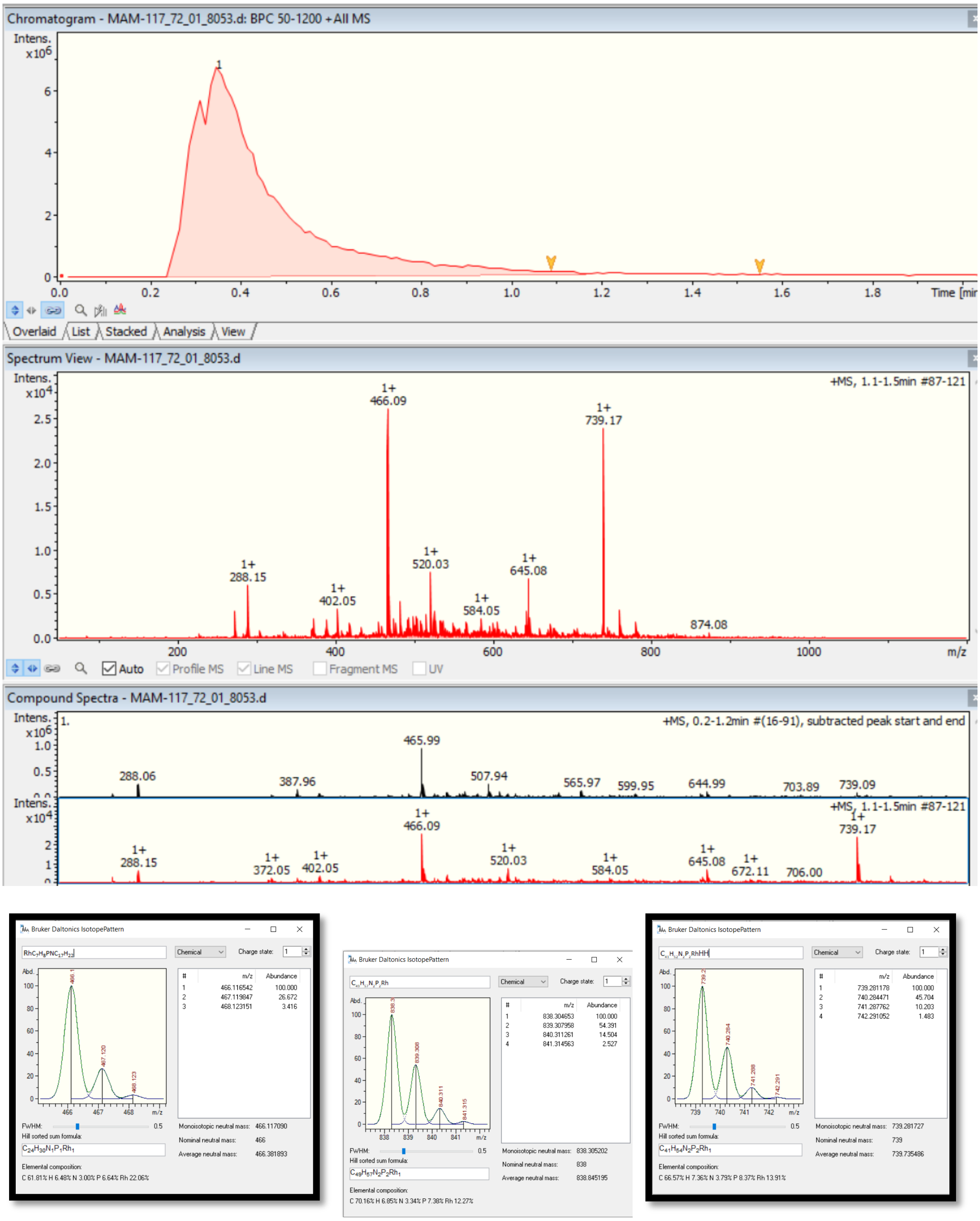

Figure S28. ESI-MS of [Rh(C≡C-Ph)(nbd){$Ph_2P(CH_2)_3NMe_2$}$_2$] (**1**) (ESI+, CH_3CN, *m/z*, %): 466.1 ([Rh(nbd){$Ph_2P(CH_2)_3NMe_2$}]$^+$, 100), 739.1 ([M - C≡C-Ph + 2H]$^+$, 90).

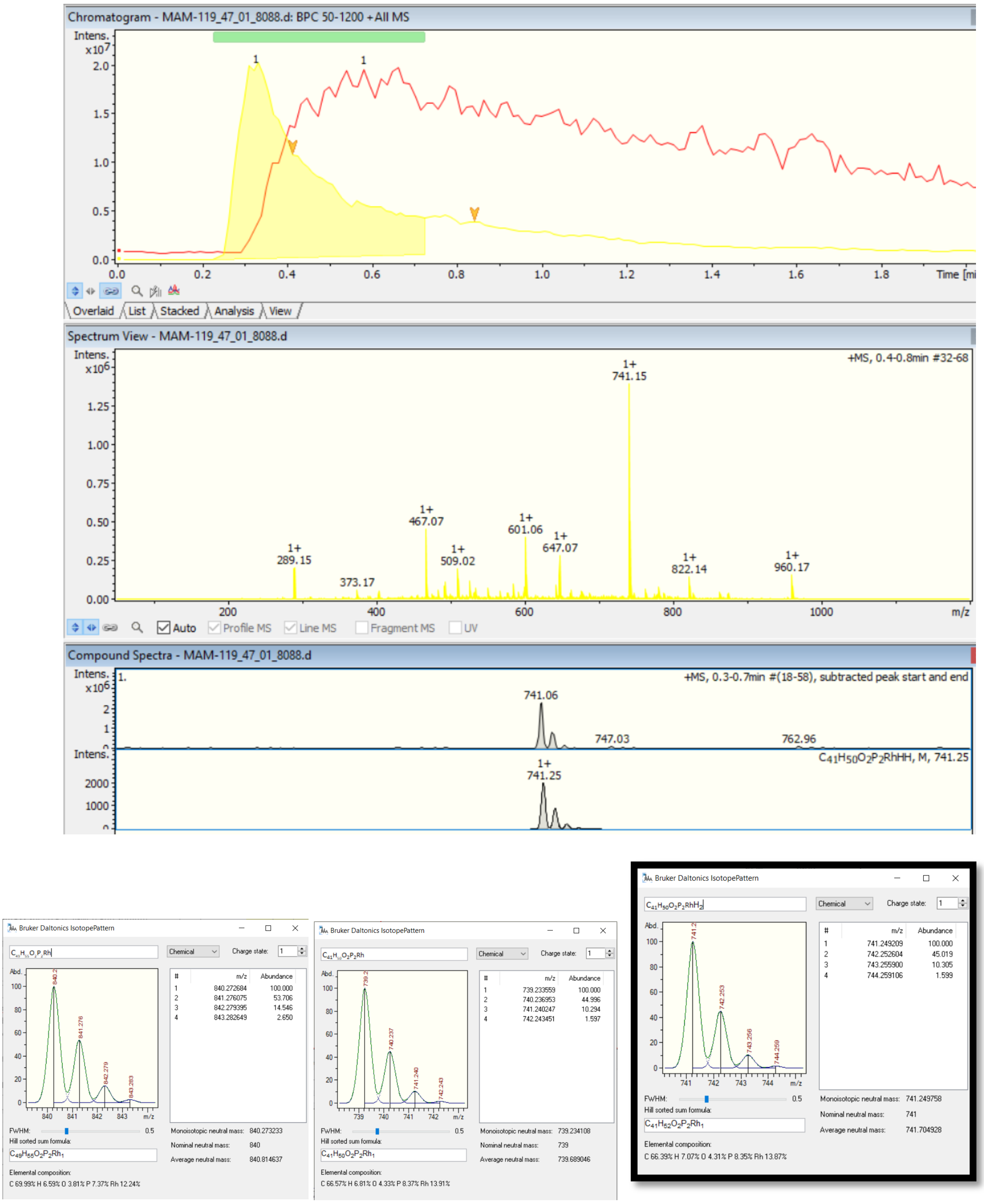

Figure S29. ESI-MS of [Rh(C≡C-Ph)(nbd){$Ph_2P(CH_2)_3OEt$}$_2$] (**2**) MS (ESI+, CH_3CN, *m/z*, %): 741.1 ([M - C≡C-Ph + 2H]$^+$, 100).

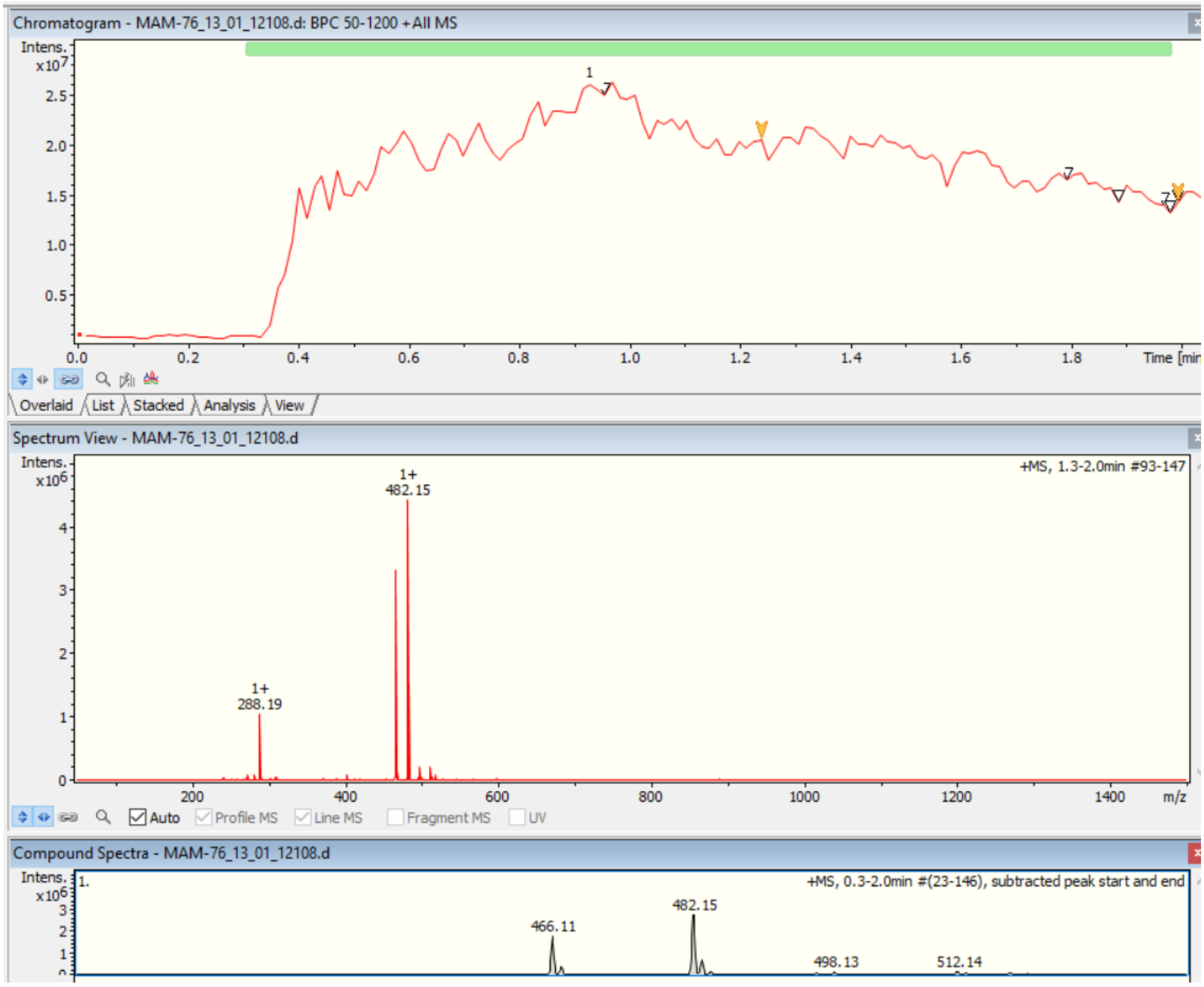

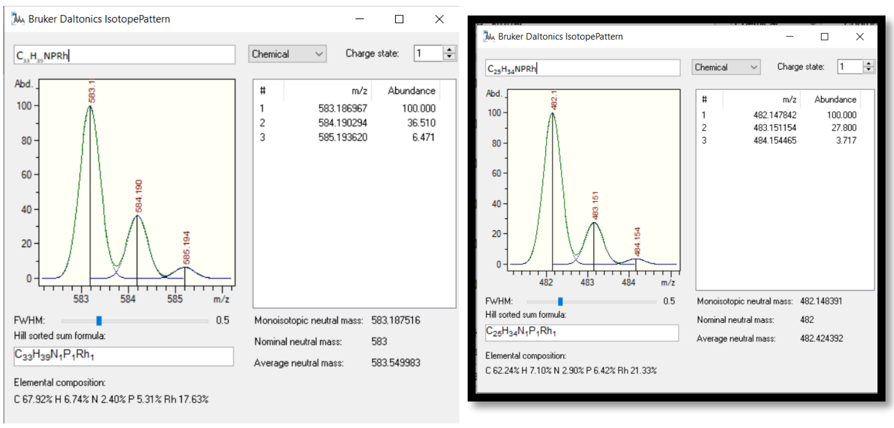

Figure S30. ESI-MS of [Rh(C≡C-Ph)(cod){$Ph_2P(CH_2)_3NMe_2$}] (**3**) (ESI+, THF, *m/z*, %): 482.1 ([M - C≡C-Ph]$^+$, 100).

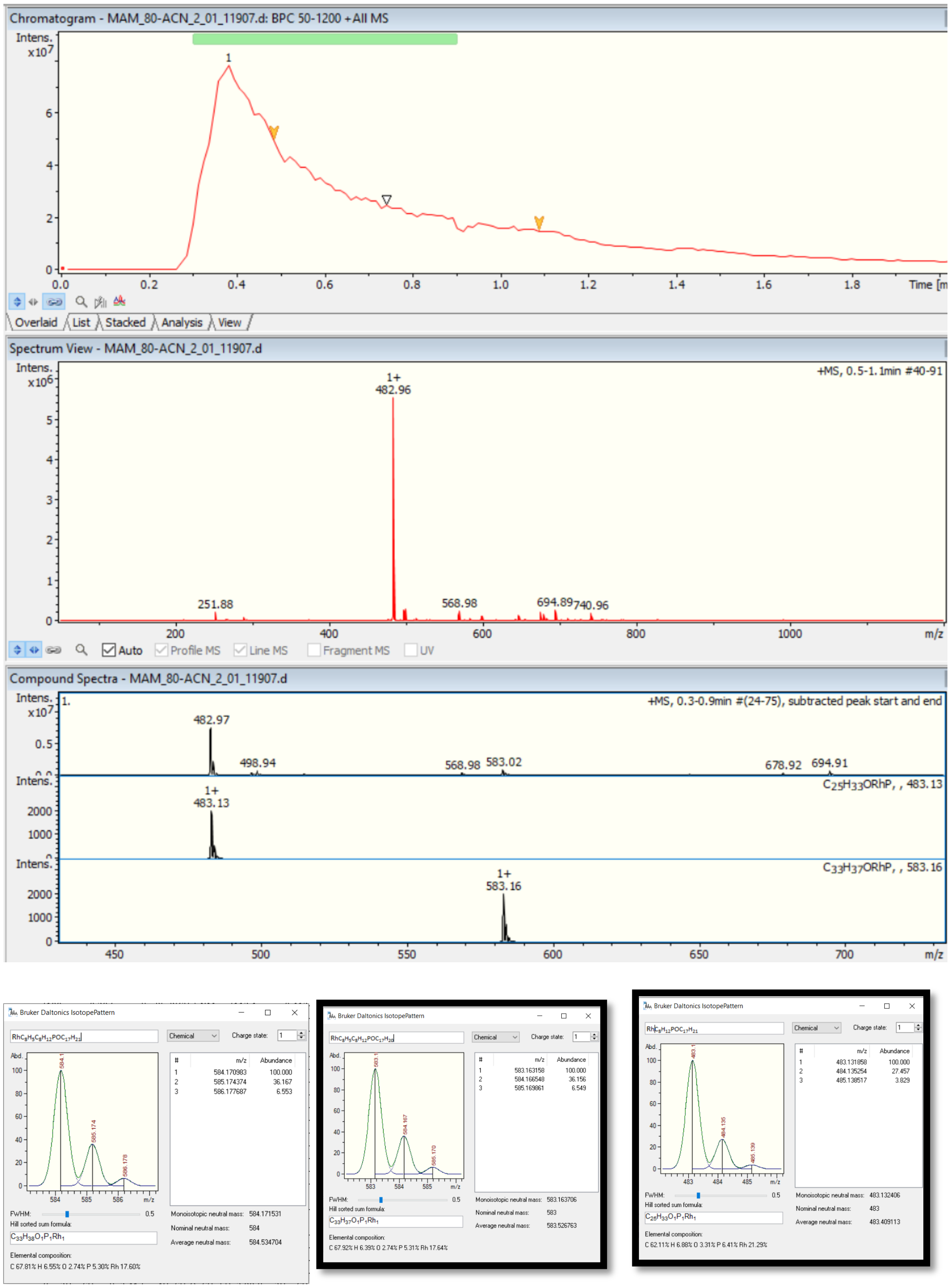

Figure S31. ESI-MS of [Rh(C≡C-Ph)(cod){$Ph_2P(CH_2)_3OEt$}] (**4**) (ESI+, THF, *m/z*, %): 583.1 ($[M]^+$, 8), 483.1 ($[M - C{\equiv}CC_6H_5]^+$, 100).

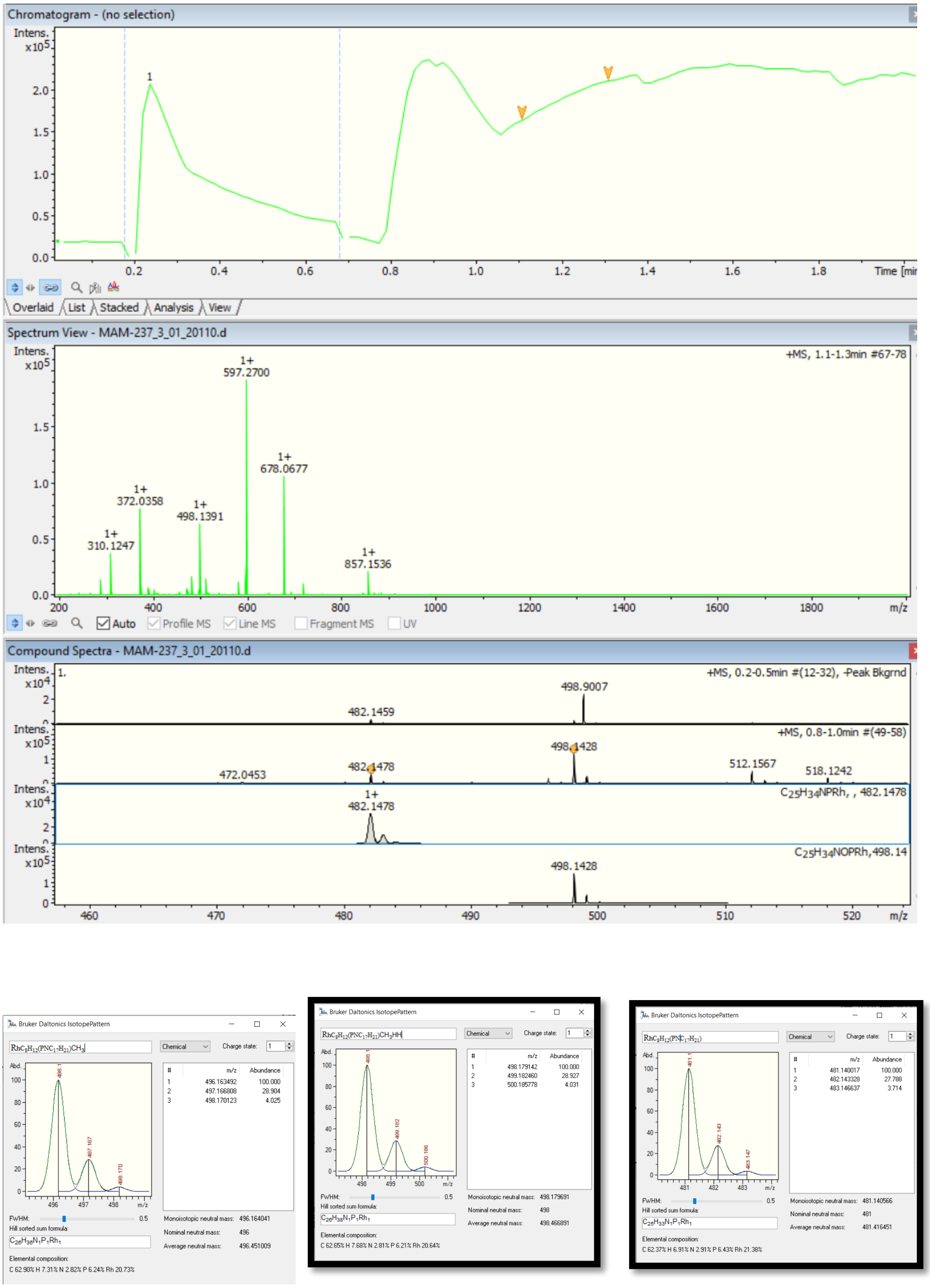

Figure S32. ESI-MS of [Rh(CH_3)(cod){$Ph_2P(CH_2)_3NMe_2$}] (**5**) (ESI+, THF, *m/z*, %): 498.1 ($[M+2H]^+$, 3), 482.1 ($[M-CH_3]^+$, 20).

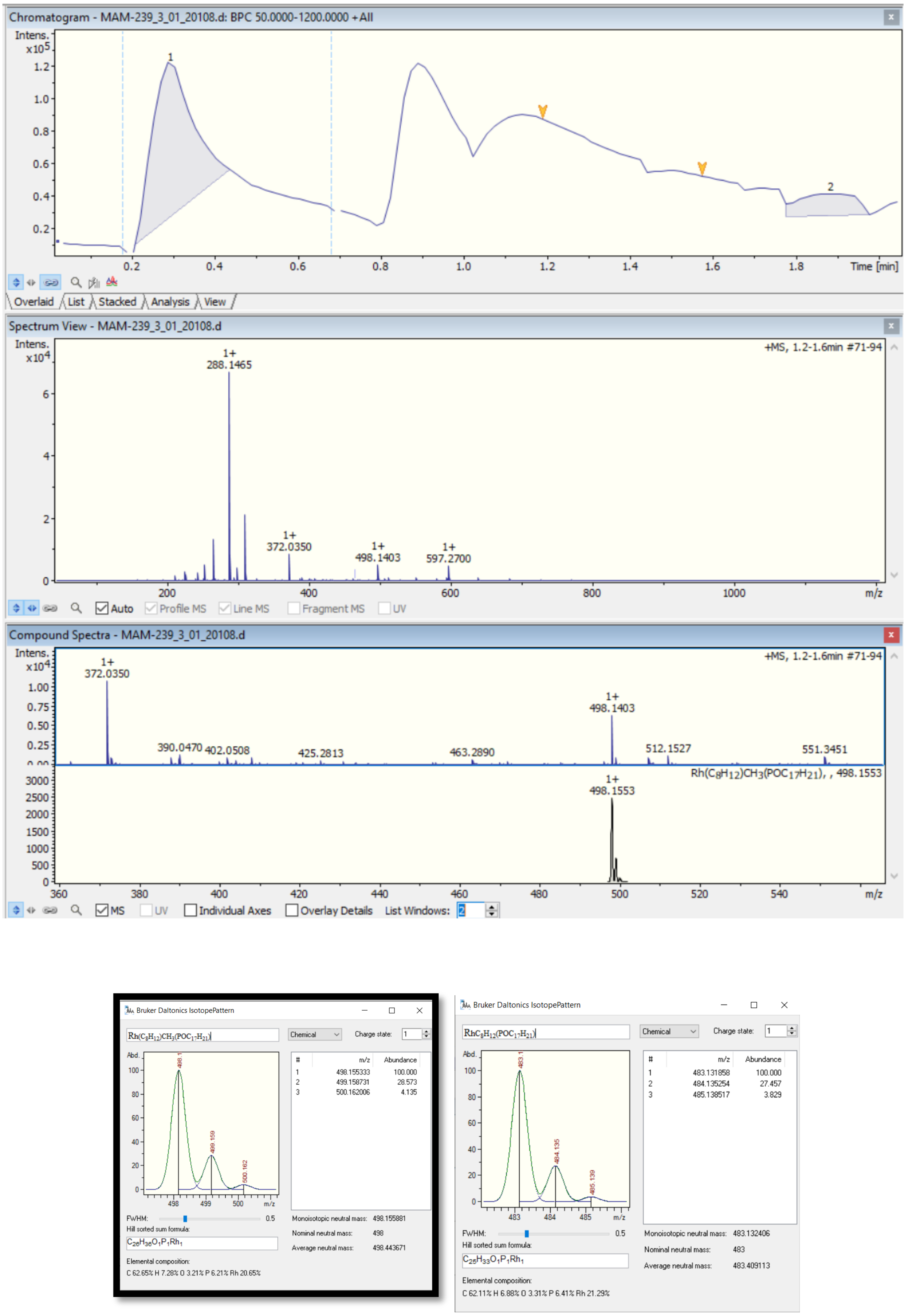

Figure S33. ESI-MS of [Rh(CH_3)(cod){$Ph_2P(CH_2)_3OEt$}] (**6**) (ESI+, THF, *m/z*, %): 498.1 ($[M]^+$, 10).

3.- Polyphenylacetylene characterization.

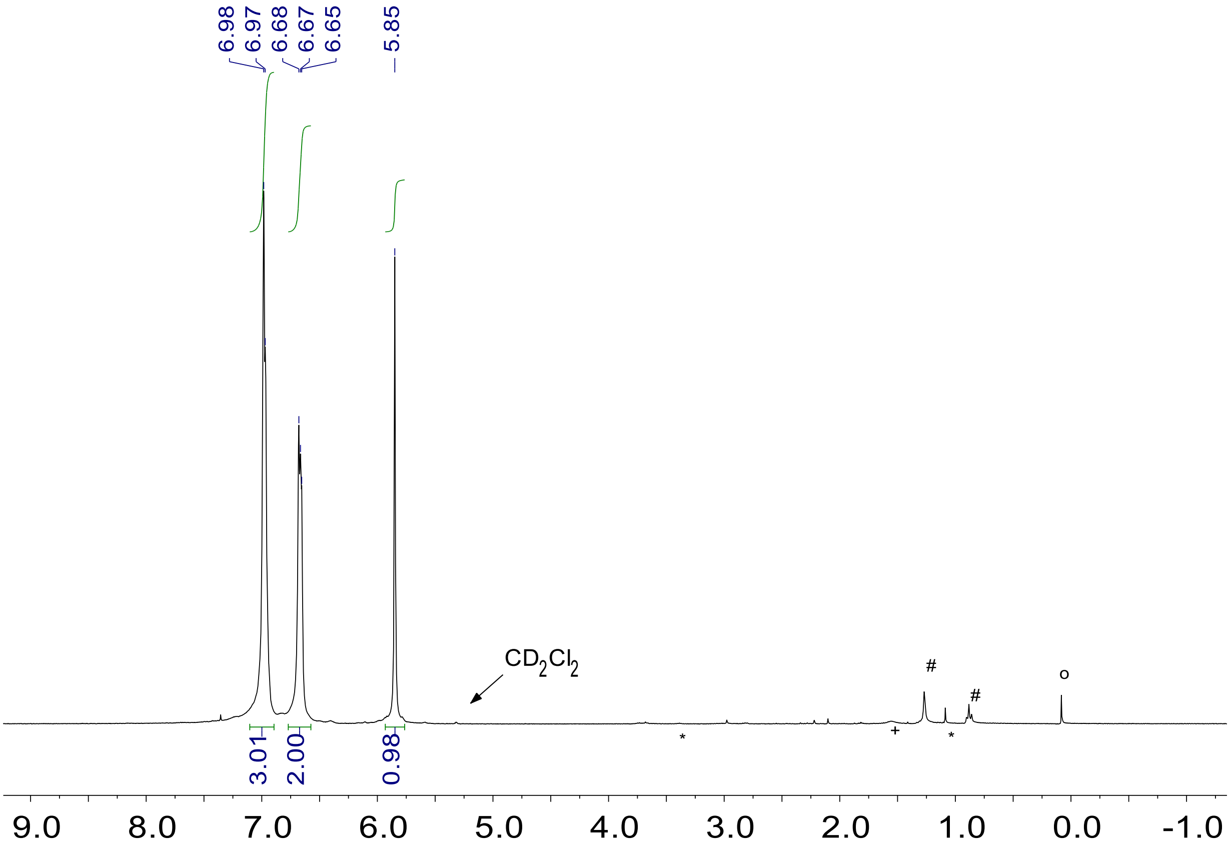

Figure S34. ^{1}H NMR (CD_2Cl_2, 298 K) of a representative PPA sample (cis-content 98 %).[1]
* methanol, + H_2O, # H grease, ○ silicone grease.[2]

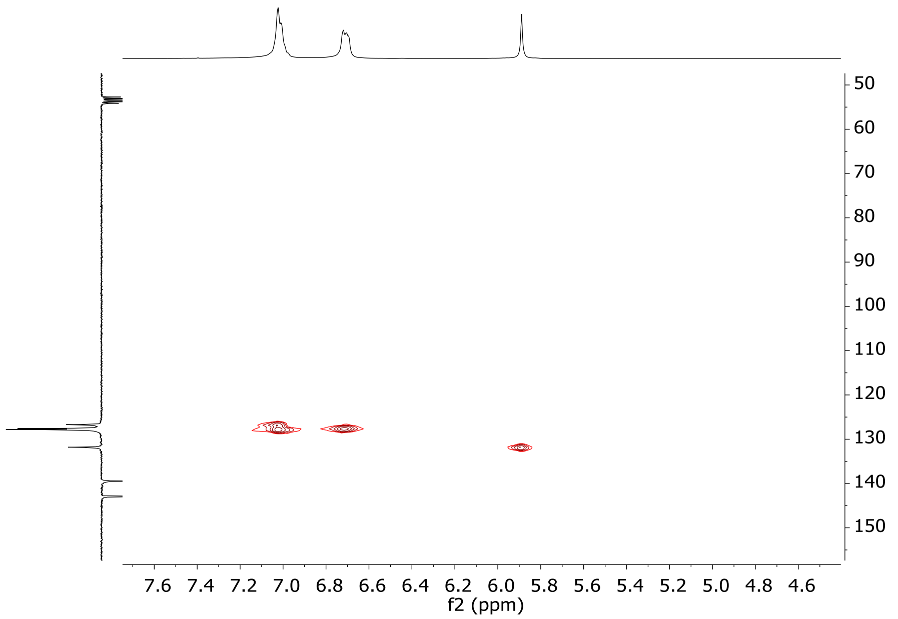

Figure S35. $^{1}H/^{13}C$ HSQC NMR (CD_2Cl_2, 298 K) of a representative PPA sample.

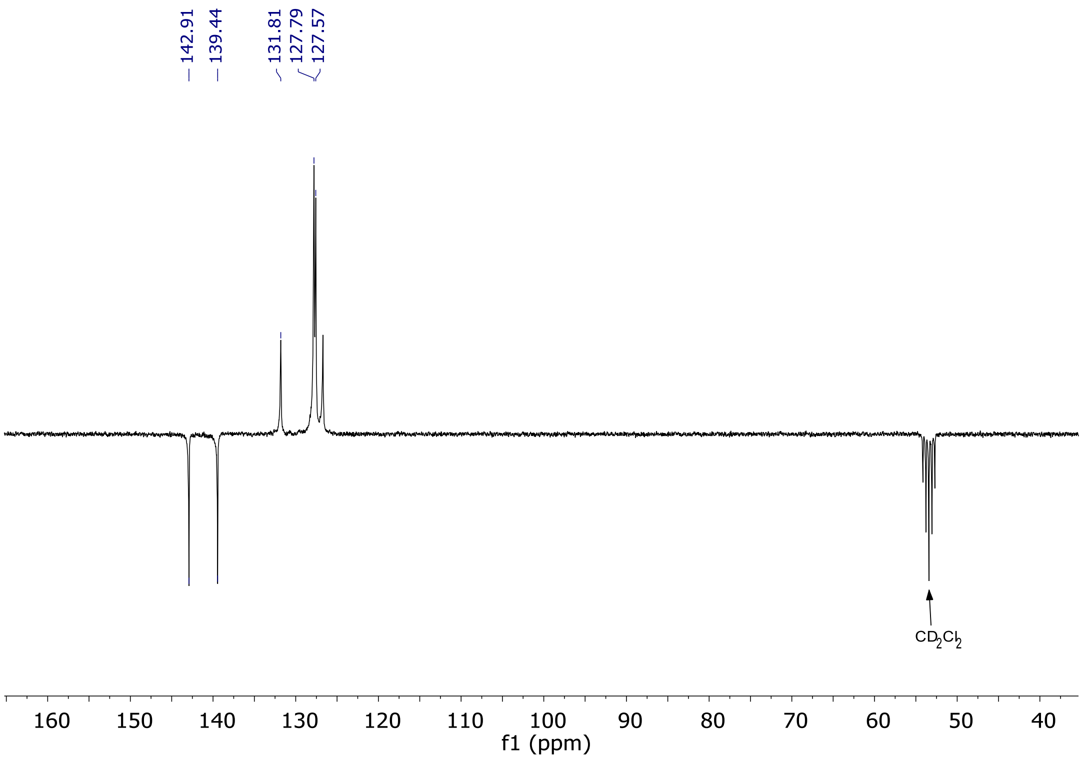

Figure S36. $^{13}C\{^1H\}$ NMR (298 K, CD_2Cl_2) of a representative PPA sample.

4.- SEC-MALS and A4F-MALS chromatograms and conformational plots of PPA samples.

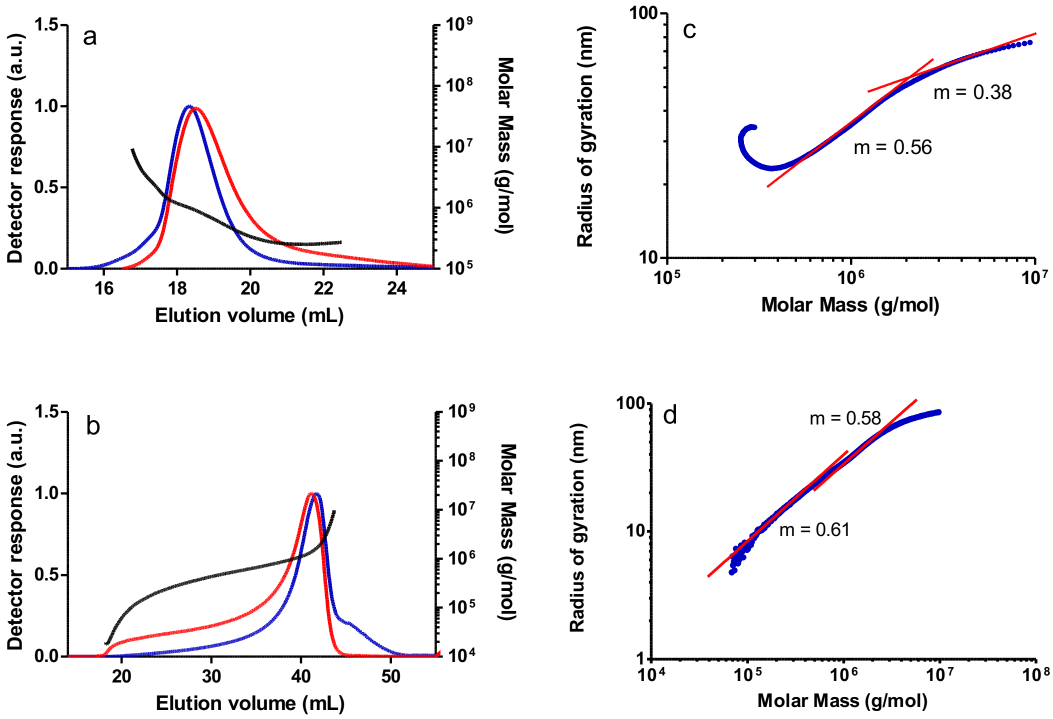

Figure S37. SEC chromatograms: light scattering detector response (90 degrees) (blue) and differential refractometer response (red), MM (molar mass) *vs*. elution volume plot for a PPA sample prepared with catalyst [Rh(C≡C-Ph)(nbd){$Ph_2P(CH_2)_3OEt$}$_2$] (**2**) in THF analyzed by: a) SEC-MALS and b) A4F-MALS. Log-log plot of the radius of gyration (r_g) vs MM (blue) and linear fit (red) of the same sample analyzed by: c) SEC-MALS and d) A4F-MALS.

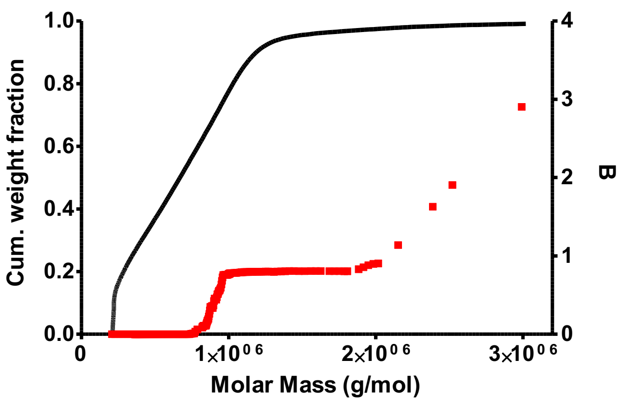

Figure S38. Cumulative molar mass distribution (black line) and branch units per macromolecule (B) (red dots) vs. MM determined by A4F-MALS for a PPA sample prepared with catalyst [Rh(C≡C-Ph)(nbd){$Ph_2P(CH_2)_3OEt$}$_2$] (**2**).

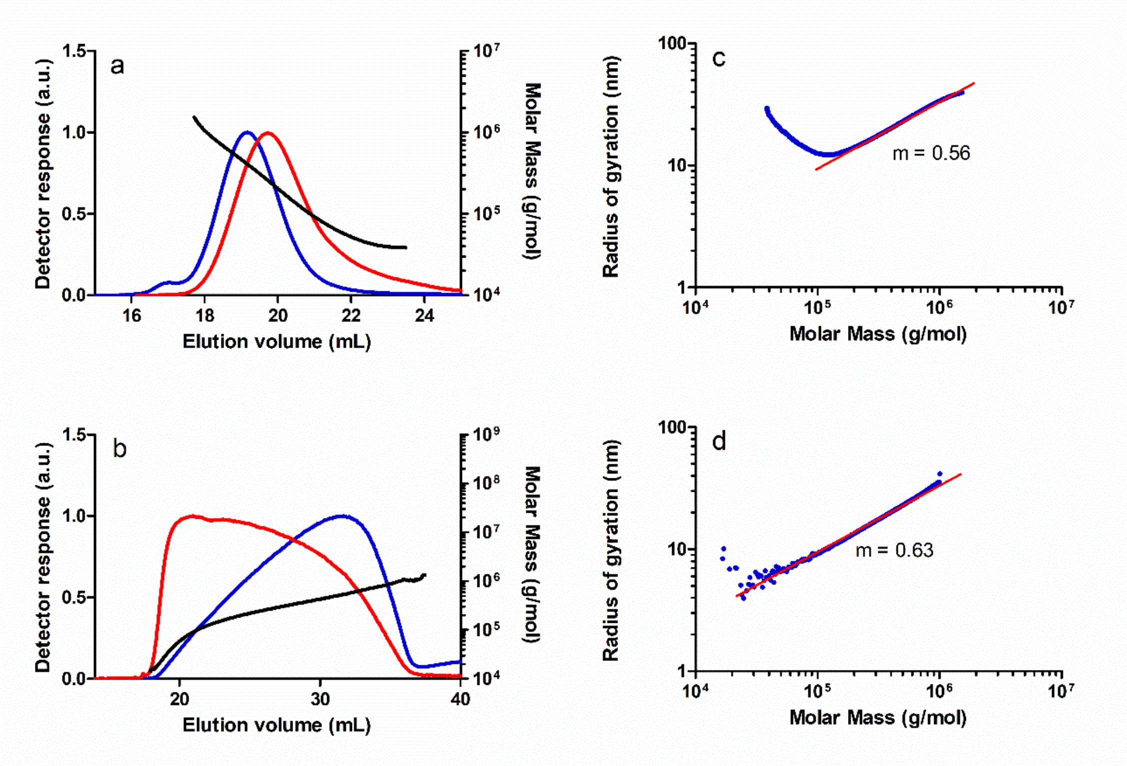

Figure S39. SEC chromatograms: light scattering detector response (90 degrees) (blue) and differential refractometer response (red), MM (molar mass) *vs*. elution volume plot for a PPA sample prepared with catalyst [Rh(C≡C-Ph)(cod){$Ph_2P(CH_2)_3NMe_2$}] (**3**) in THF analyzed by: a) SEC-MALS and b) A4F-MALS. Log-log plot of the radius of gyration (r_g) vs MM (blue) and linear fit (red) of the same sample analyzed by: c) SEC-MALS and d) A4F-MALS.

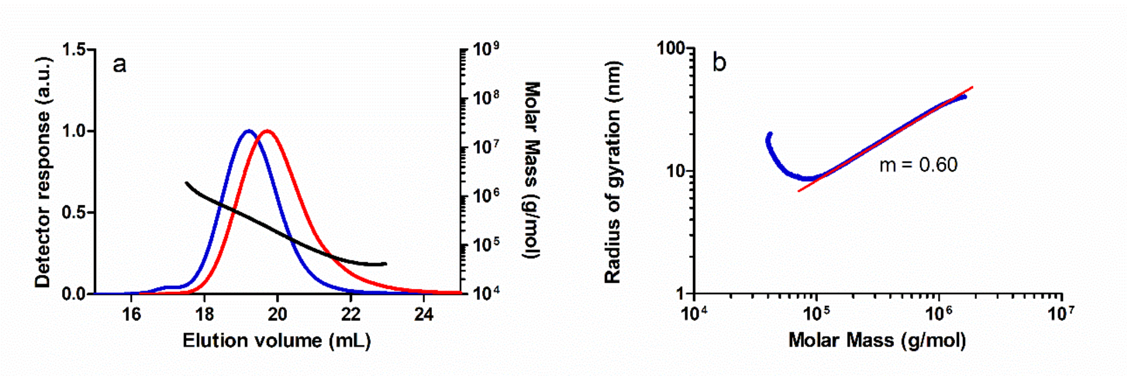

Figure S40. a) SEC chromatograms: light scattering detector response (90 degrees) (blue) and differential refractometer response (red), MM (molar mass) *vs*. elution volume plot for a PPA sample prepared with catalyst [Rh(CH_3)(cod){$Ph_2P(CH_2)_3OEt$}] (**6**) in THF analyzed by SEC-MALS and b) Log-log plot of the radius of gyration (r_g) vs MM of the same sample analyzed by SEC-MALS (blue) and linear fit (red).

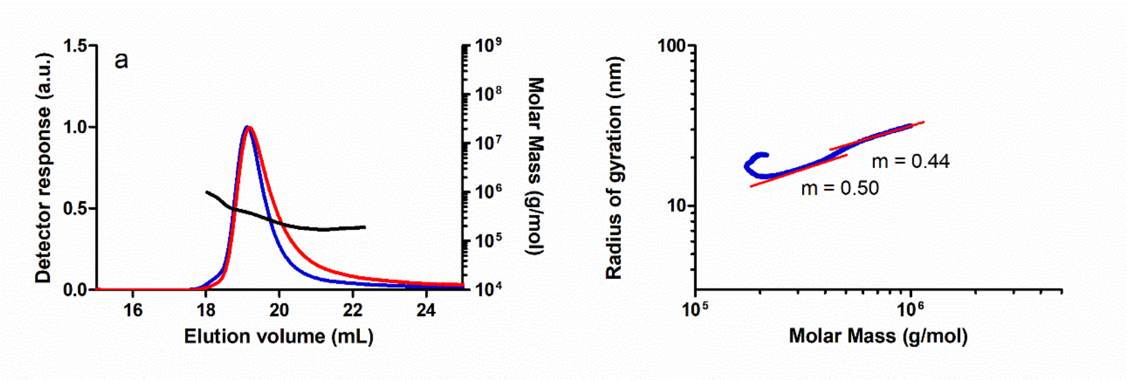

Figure S41. a) SEC chromatograms: light scattering detector response (90 degrees) (blue) and differential refractometer response (red), MM (molar mass) *vs*. elution volume plot for a PPA sample prepared with catalyst [Rh(C≡CC_6H_5)(nbd){$Ph_2P(CH_2)_3NMe_2$}$_2$] (**1**)/DMAP in THF analyzed by SEC-MALS and b) Log-log plot of the radius of gyration (r_g) vs MM of the same sample analyzed by SEC-MALS (blue) and linear fit (red).

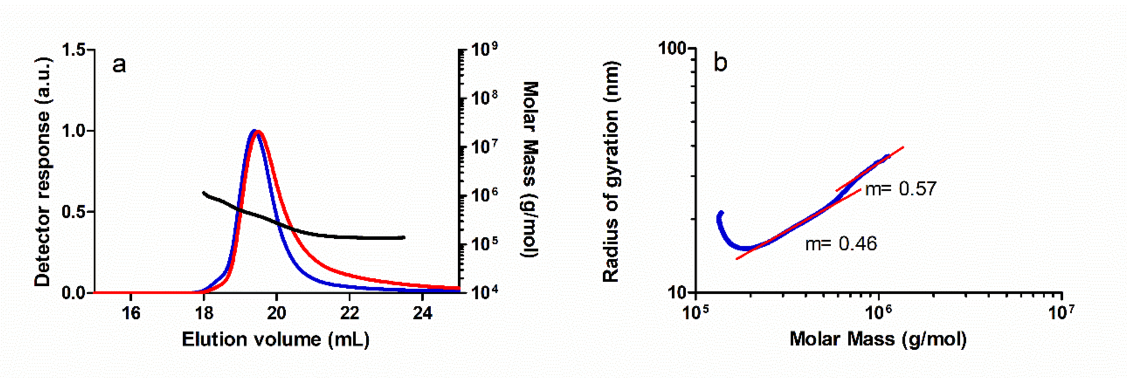

Figure S42. a) SEC chromatograms: light scattering detector response (90 degrees) (blue) and differential refractometer response (red), MM (molar mass) *vs*. elution volume plot for a PPA sample prepared with catalyst [Rh(C≡CC_6H_5)(nbd){$Ph_2P(CH_2)_3OEt$}$_2$] (**2**)/DMAP in THF analyzed by SEC-MALS and b) Log-log plot of the radius of gyration (r_g) vs MM of the same sample analyzed by SEC-MALS (blue) and linear fit (red).

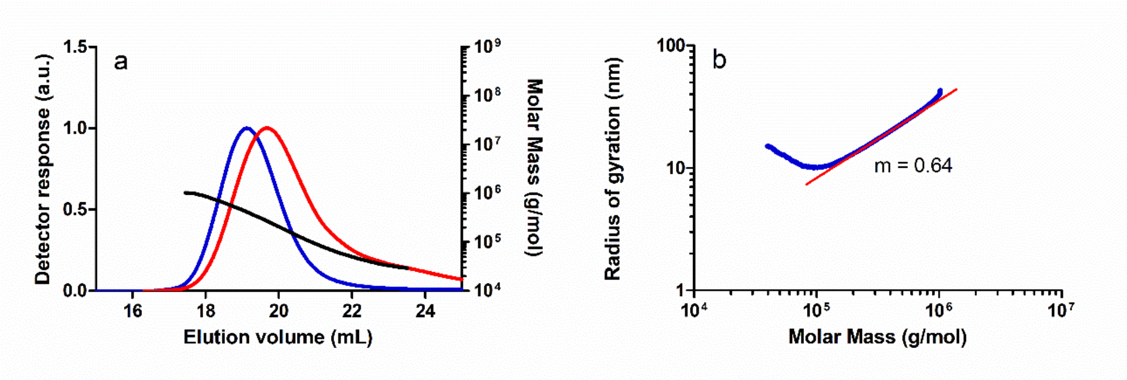

Figure S43. a) SEC chromatograms: light scattering detector response (90 degrees) (blue) and differential refractometer response (red), MM (molar mass) *vs*. elution volume plot for a PPA sample prepared with catalyst [Rh(C≡CC_6H_5)(cod){$Ph_2P(CH_2)_3NMe_2$}] (**3**)/DMAP in THF analyzed by SEC-MALS and b) Log-log plot of the radius of gyration (r_g) vs MM of the same sample analyzed by SEC-MALS (blue) and linear fit (red).

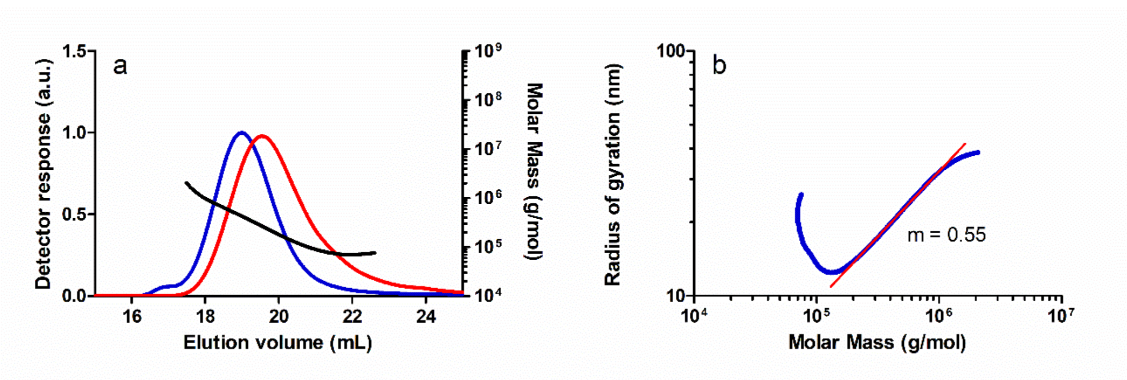

Figure S44. a) SEC chromatograms: light scattering detector response (90 degrees) (blue) and differential refractometer response (red), MM (molar mass) *vs*. elution volume plot for a PPA sample prepared with catalyst [Rh(C≡C-Ph)(cod){$Ph_2P(CH_2)_3OEt$}] (**4**)/DMAP in THF analyzed by SEC-MALS and b) Log-log plot of the radius of gyration (r_g) vs MM of the same sample analyzed by SEC-MALS (blue) and linear fit (red).

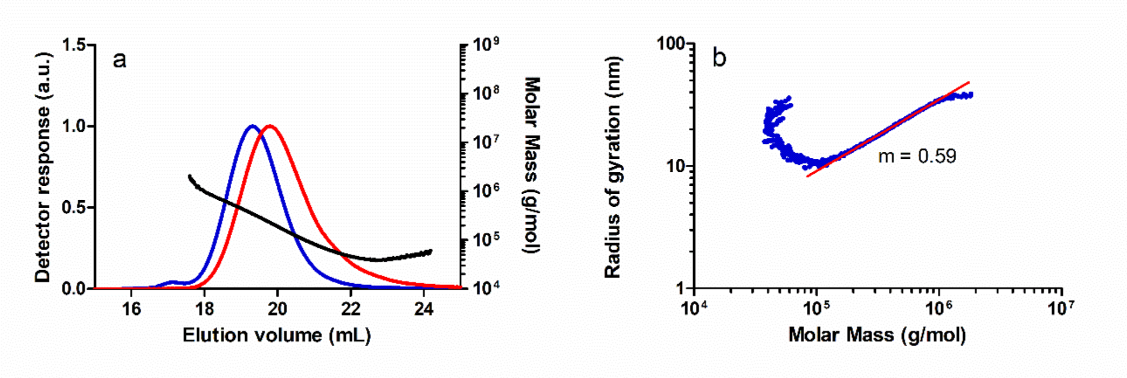

Figure S45. a) SEC chromatograms: light scattering detector response (90 degrees) (blue) and differential refractometer response (red), MM (molar mass) *vs*. elution volume plot for a PPA sample prepared with catalyst [Rh(cod){κ^2*P*,*N*-$Ph_2P(CH_2)_3NMe_2$}]BF_4] (**7**) in THF analyzed by SEC-MALS and b) Log-log plot of the radius of gyration (r_g) vs MM of the same sample analyzed by SEC-MALS (blue) and linear fit (red).

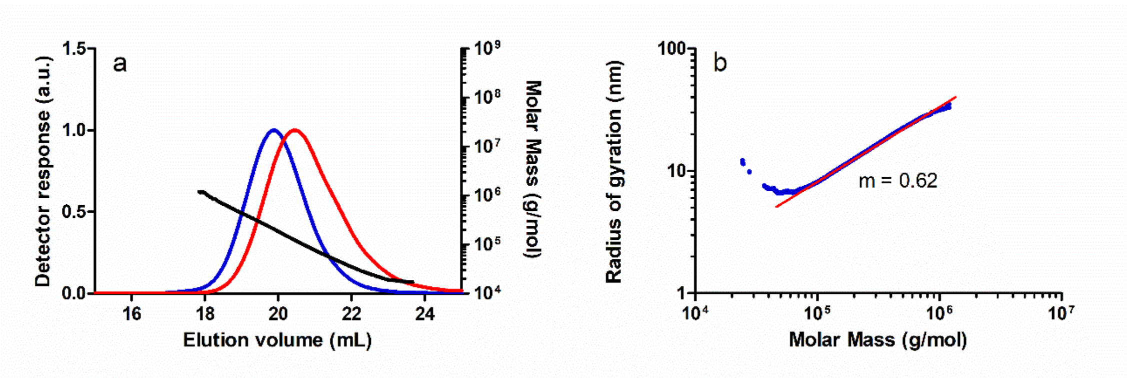

Figure S46. a) SEC chromatograms: light scattering detector response (90 degrees) (blue) and differential refractometer response (red), MM (molar mass) *vs*. elution volume plot for a PPA sample prepared with catalyst [Rh(cod){κ^2*P*,*O*-$Ph_2P(CH_2)_3OEt$}]BF_4 (**8**) in THF analyzed by SEC-MALS and b) Log-log plot of the radius of gyration (r_g) vs MM of the same sample analyzed by SEC-MALS (blue) and linear fit (red).

5.- Possible branching mechanisms.

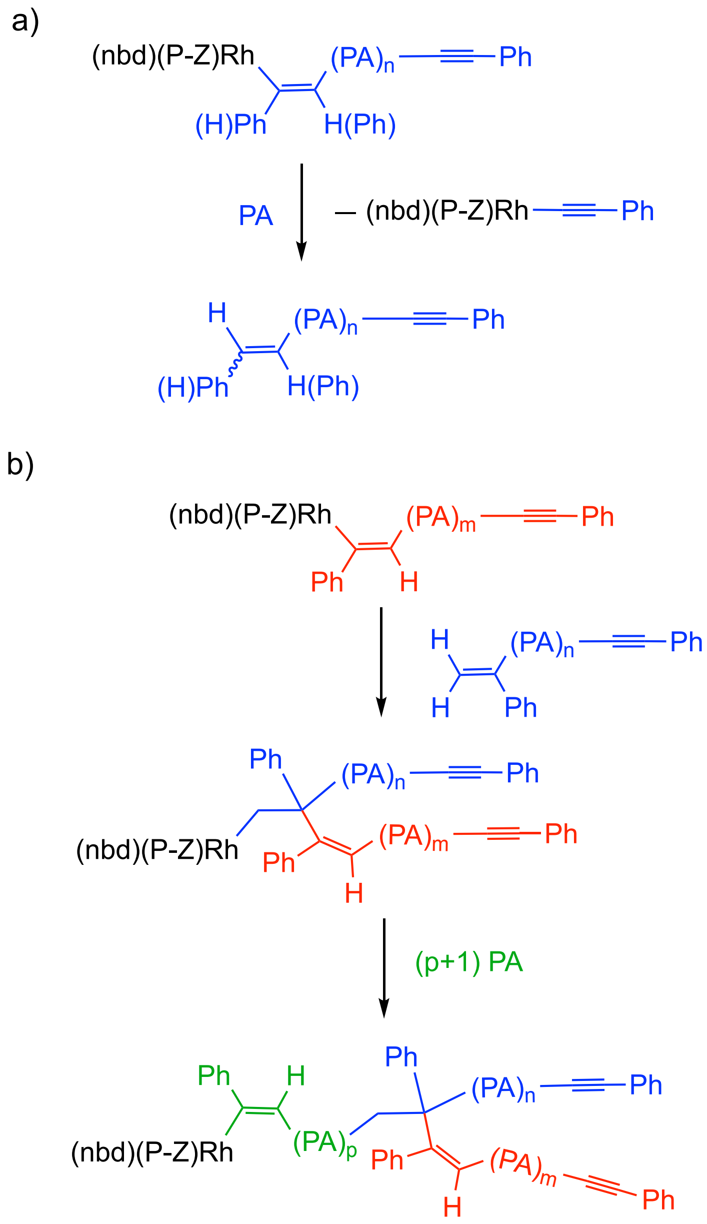

P-Z = $Ph_2P(CH_2)_3Z$ (Z = NMe_2, OEt)

Figure S47. Terminal branching: a) Chain transfer to PA leading to the formation of a macromonomer with vinylene or vinylidene end groups. b) Macromonomer copolymerization leading to terminal branching.

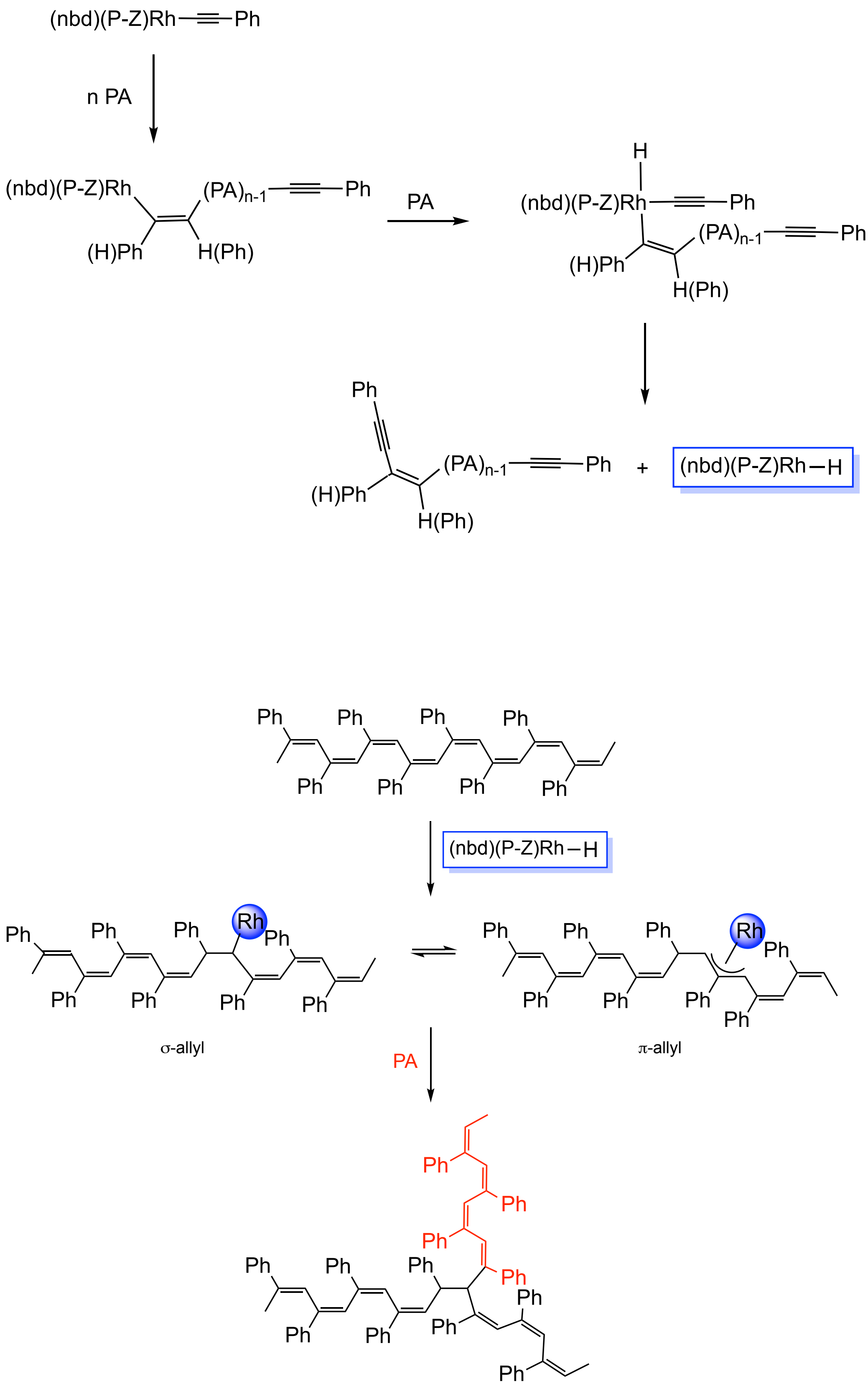

Figure S48. Formal chain transfer to polymer mechanism leading to branch formation.

6.- References

1.- The % cis content in cis-transoidal PPA samples was determined using the following equation: % cis = 100 ($A_{5.85}$ x 6)/(A_{total}) where $A_{5.85}$ is the area of the vinyl proton and A_{total} is the total area of the spectrum. a) A. Furlani, C. Napoletano, M. V. Russo and W. Feast, Stereoregular polyphenylacetylene, *J. Polym. Bull.*, 1986, **16**, 311–317. b) A. Furlani, C. Napoletano, M. V. Russo, A. Camus and N. J. Marsich, The influence of the ligands on the catalytic activity of a series of RhI complexes in reactions with phenylacetylene: Synthesis of stereoregular poly(phenyl) acetylene, *Polym. Sci., Part A: Polym. Chem.*, 1989, **27**, 75–86.

2.- G. R. Fulmer, A. J. M. Miller, N. H. Sherden, H. E. Gottlieb, A. Nudelman, B. M. Stoltz, J. E. Bercaw, K. I. Goldberg, NMR Chemical Shifts of Trace Impurities: Common Laboratory Solvents, Organics, and Gases in Deuterated Solvents Relevant to the Organometallic Chemist, *Organometallics* 2010, **29**, 2176–2179.